1   **Title: The molecular mechanism and physiological role of silent nociceptor**

2   **activation.**

3

4   **Author list**

5   Timo A. Nees[1,2], Na Wang[1], Pavel Adamek[3], Clement Verkest[3], Carmen La Porta[1],

6   Irina Schaefer[1], Julie Virnich[3], Selin Balkaya[3], Vincenzo Prato[1], Chiara Morelli[4], Nadja

7   Zeitzschel[3], Valerie Begay[5], Young Jae Lee[6], Anke Tappe-Theodor[1], Gary R. Lewin[5],

8   Paul A. Heppenstall[4], Francisco J. Taberner[1,7], Stefan G. Lechner[1,3,*]

9

10 **Affiliations**

11 [1] Institute of Pharmacology, Heidelberg University, Im Neuenheimer Feld 366, 69120

12 Heidelberg, Germany

13 [2] Clinic for Orthopedics and Trauma Surgery, Center for Orthopedics, Trauma

14 Surgery and Spinal Cord Injury, Heidelberg University Hospital, Schlierbacher

15 Landstrasse 200a, 69118 Heidelberg, Germany

16 [3] Department of Anesthesiology, University Medical Center Hamburg-Eppendorf,

17 Martinistrasse 52, 20246 Hamburg, Germany

18 [4] SISSA: Scuola Internazionale Superiore di Studi Avanzati, Via Bonomea, 265,

19 34136 Trieste, Italy.

20 [5] Department of Neuroscience, Max Delbrück Center for Molecular Medicine, Berlin,

21 Germany.

22 [6] Department of Biochemistry, Lee Gil Ya Cancer and Diabetes Institute, Gachon

23 University College of Medicine, Incheon, Republic of Korea

24 [7] Instituto de Neurosciencias de Alicante, Universidad Miguel Hernández – CSIC,

25 Alicante, Spain

26

27 ***Corresponding Author:**

28 Stefan G. Lechner

29 Department of Anesthesiology, University Medical Center Hamburg-Eppendorf

30 Martinistrasse 52, 20246 Hamburg, Germany

31 Phone: +49-(0)40-7410 53480

32 Email: s.lechner@uke.de

33

Summary

Silent nociceptors are sensory afferents that are insensitive to noxious mechanical stimuli under normal conditions but become sensitized to such stimuli during inflammation. Using RNA-sequencing and quantitative RT-PCR we demonstrate that inflammation selectively upregulates the expression of the transmembrane protein TMEM100 in silent nociceptors and electrophysiology revealed that over-expression of TMEM100 is required and sufficient to un-silence silent nociceptors. Moreover, we show that mice lacking TMEM100 do not develop secondary allodynia – i.e. pain hypersensitivity that spreads beyond the site of inflammation – in a mouse model of knee joint inflammation and that AAV-mediated overexpression of TMEM100 in articular afferents in the absence of inflammation is sufficient to induce allodynia in remote skin regions without causing knee joint pain. Thus, our work identifies TMEM100 as a key regulator of silent nociceptor un-silencing and reveals a physiological role for this hitherto enigmatic afferent subclass in triggering spatially remote secondary allodynia during inflammation.

Introduction

Pain is an unpleasant and multifaceted sensation that can be stabbing, burning, throbbing or prickling. Likewise, pain hypersensitivity has many faces and can manifest as increased sensitivity to heat, cold or mechanical stimuli that commonly spreads far beyond the site of initial insult, a phenomenon known as secondary hyperalgesia or allodynia. Our ability to distinguish this plethora of painful sensations, relies on the functional diversity of primary sensory afferents, which detect painful stimuli and relay information about the intensity and quality of these stimuli to the central nervous system. Functionally distinct subclasses of sensory afferents have already been discovered several decades ago by classical neurophysiological studies [1] and, more recently, single-cell RNA-sequencing studies have mapped transcriptional signatures to these functionally classified neurons [2,3] and revealed changes therein associated with chronic pain [4,5]. Moreover, knock-out, cell ablation and optogenetic studies have deciphered the contribution of various afferent subclasses to different forms of pain, such as acute pain evoked by pinprick, pinch and punctate mechanical stimuli as well as mechanical allodynia and cold allodynia associated with nerve injury [6–10].

Despite the clear picture regarding the contribution of different primary afferent subtypes to various forms of pain that has emerged during the past decade, the function of one of the largest subpopulations of nociceptors – the so-called 'silent' nociceptors – still remains enigmatic. The term 'silent' nociceptor denotes sensory afferents that do not respond to noxious mechanical stimuli under normal conditions but become sensitized to such stimuli during experimentally induced inflammation. Silent nociceptors were first documented in the articular nerves of the cat knee joint [11] and were subsequently found in the colon [12,13] and the bladder [14] as well as in human skin [15]. Since the sensitivity of silent nociceptors to non-mechanical stimuli has never been systematically tested, it is, however, more appropriate to use the term mechanically insensitive afferents (MIAs) to describe this peculiar afferent subclass. It is estimated that MIAs constitute ~30% of all C-fiber afferents in viscera and joints and about 15-20% in the human skin, whereas they appear to be less abundant in mouse skin [16,17]. Considering the large proportion of MIAs in viscera and joints, it has been hypothesized that the un-silencing of MIAs during inflammation substantially increases nociceptive input onto the spinal cord, which supposedly potentiates central pain processing and eventually results in increased pain sensitivity. Microneurography from cutaneous human afferents, on the other hand, suggested that silent nociceptors might

3

1   induce secondary mechanical hyperalgesia [18]. Owing to the lack of tools that would

2   allow the unequivocal identification or the selective genetic manipulation of MIAs,

3   neither the mechanism underlying the un-silencing of MIAs nor their exact role in pain

4   signaling have hitherto been deciphered.

5   We had previously shown that mouse MIAs express the nicotinic acetylcholine receptor

6   alpha-3 subunit (CHRNA3) and can thus readily be identified in Tg(Chrna3-

7   EGFP)BZ135Gsat reporter mice [19]. Most importantly, we had shown that CHRNA3-

8   EGFP$^+$ MIAs acquire mechanosensitivity upon treatment with the inflammatory

9   mediator nerve growth factor (NGF) and demonstrated that this process requires de-

10 novo gene transcription. We thus here set out to identify transcriptional changes that

11 underlie the un-silencing of CHRNA3-EGFP$^+$ MIAs and to eventually utilize these

12 findings to examine the contribution of MIAs to the generation of inflammatory pain.

13

Results

NGF treatment selectively upregulates TMEM100 in silent nociceptors

16 To identify proteins required for the NGF-induced acquisition of mechanosensitivity of

17 CHRNA3-EGFP$^+$ MIAs [19], we compared the transcriptomes of CHRNA3-EGFP$^+$

18 neurons, cultured in the absence or presence of NGF (50 ng/ml) for 24 h, using paired-

19 end RNAseq (Fig. 1a). This comparison showed that neither the mechanically-gated

20 ion channel PIEZO2, which is required for mechanotransduction in CHRNA3-EGFP$^+$

21 neurons [19], nor any of the known PIEZO2 modulators, such as *Stoml3*, *Pcnt*, *Mtmr2*,

22 *Tmem150c*, *Cdh1*, *Anxa6*, *Atp2a2* and *Nedd4-2* [20–27], are up-regulated by NGF (Fig.

23 1b). Moreover, the analysis showed that CHRNA3-EGFP$^+$ MIAs have a transcriptional

24 signature – i.e. co-expression of *Ntrk1, Calca, Tac1, Trpv1, Nos1, Ly6e* and *Htr3a* but

25 not *Cyp2j12, Prrx2* and *Etv1* (Fig. 1c) – that was previously observed in a subset of

26 peptidergic nociceptors that were classified as PSPEP2 neurons in a large scale

27 single-cell RNA-sequencing study [2]. Most importantly, the RNAseq screen revealed

28 the NGF-induced up-regulation of the transmembrane protein TMEM100 (fold-

29 change=3.805, P=4.12E-5, N=3 samples per condition, Fig. 1b), which attracted our

30 attention because TMEM100 was previously shown to potentiate the activity of TRPA1

31 [28] – an ion channel that plays an important role in pain signaling [29] – by releasing it

32 from the inhibition by TRPV1 and both channels are expressed at significant levels in

33 CHRNA3-EGFP$^+$ neurons (Fig. 1c, d). Importantly, quantitative real-time PCR (qPCR)

34 confirmed the up-regulation of TMEM100 in CHRNA3-EGFP$^+$ MIAs and further showed

1   that no other major nociceptor subpopulation exhibits significant changes in TMEM100

2   expression upon NGF treatment (Fig. 1e).

3   We thus next asked if the up-regulation of TMEM100 is involved in the acquisition of

4   mechanosensitivity in MIAs. To this end we compared mechanotransduction currents

5   from control and TMEM100-overexpressing CHRNA3-EGFP⁺ DRG neurons using an

6   electrophysiological approach known as the mechano-clamp technique [30]. Here,

7   transmembrane currents are recorded from cultured DRG neurons in the whole-cell

8   configuration of the patch-clamp technique while the cell soma is mechanically

9   stimulated with a fire-polished patch-pipette. Consistent with our previous results [19],

10   only a small proportion of un-transfected CHRNA3-EGFP⁺ cells (3/14) responded to

11   mechanical stimulation with small inward currents (Fig. 1f – h). Strikingly, however,

12   ~61% of the CHRNA3-EGFP⁺ neurons transfected with TMEM100 exhibited robust

13   mechanotransduction currents that were significantly bigger than the small currents

14   occasionally observed in control cells (Fig. 1g and h). When expressed in HEK293

15   cells, TMEM100 did not produce mechanotransduction currents and did not modulate

16   PIEZO2 mediated currents in these cells (Supplementary Fig. 1), indicating that

17   TMEM100 is neither a channel itself nor a modulator of PIEZO2, but solely un-silences

18   PIEZO2 in the specific cellular context of CHRNA3-EGFP⁺ MIAs.

19

20   **Intraarticular CFA injection induces knee joint pain and secondary allodynia in**

21   **remote skin regions**

22   To corroborate our in-vitro observations, we next examined the role of TMEM100 in

23   the sensitization of MIAs in an *in-vivo* mouse model of Complete Freund's adjuvant

24   (CFA)-induced knee joint monoarthritis. We chose knee joint inflammation as the

25   experimental model because (i) MIAs were shown to constitute ~50% of all articular

26   nociceptive afferents [11,19], (ii) because the levels of NGF, which induces up-regulation

27   of TMEM100, are significantly increased in synovial fluid in rodent models of

28   inflammatory knee joint pain as well as in patients with osteoarthritis [31,32] and (iii)

29   because anti-NGF antibodies alleviate joint pain in patients with osteoarthritis [33],

30   suggesting that NGF and possibly MIAs, may play an important role in the generation

31   of knee joint pain.

32   Consistent with our previous study [19], we found that the knee joint is densely innervated

33   by CHRNA3-EGFP⁺ afferents that co-express calcitonin gene-related peptide (CGRP),

34   which mostly terminate in Hoffa's fat pad (Fig. 2a – c). As previously described [34],

1   intraarticular CFA injection caused prominent knee joint inflammation characterized by

2   redness and swelling (Fig. 2d), which was accompanied by severe limping

3   (Supplementary Movies S1 and S2) – indicative of primary hyperalgesia in the knee –

4   and by secondary mechanical and thermal hypersensitivity in skin regions remote from

5   the knee joint. Primary knee joint hyperalgesia was quantified with the Catwalk XT gait

6   analysis system (Fig. 2e), which revealed that mice with an inflamed knee joint put less

7   weight on the affected leg, evidenced by a reduction of the ratio of the foot print area

8   of the ipsi- (left) and contralateral (right) hind paw (before, 1.07 ± 0.03 vs. 3 days post

9   injection (dpi) CFA, 0.57 ± 0.07, N=16, Students paired t-test, P= $2.6*10^{-7}$), and a

10   reduction of the leg swing speed of the inflamed leg (before, 1.041 ± 0.017 vs. 3 dpi

11   CFA, 0.634 ± 0.044, N=16, Students paired t-test, P= $8*10^{-9}$; Fig. 2f). Secondary

12   mechanical and thermal hypersensitivity was assessed in the ipsilateral hind paw using

13   the von Frey and Hargreaves tests, respectively. These tests showed that CFA-

14   induced monoarthritis, reduces the minimal force of punctate mechanical stimuli –

15   applied with von Frey filaments to the plantar surface of the hind paw – required to

16   evoked a paw withdrawal reflex from 0.87 ± 0.03 g before to 0.15 ± 0.03 g three days

17   post CFA injection (Student's paired t-test, P=$5.18*10^{-12}$; Fig. 2g). Likewise, the

18   latencies of paw withdrawals evoked by heat stimulation of the hind paw were also

19   significantly reduced (before, 6.03 ± 0.28 s vs. 3 dpi CFA 2.31 ± 0.11 s N=16, Student's

20   paired t-test, P=$1.8*10^{-9}$, Fig. 2h).

21

CFA-induced knee joint inflammation induces mechanosensitivity and
22
potentiates TRPA1 activity in CHRNA3-EGFP⁺ afferents
23

24   To enable the examination of CFA-induced transcriptional and functional changes in

25   MIAs, we next back-labelled sensory neurons that give rise to articular afferents by

26   intraarticular injection of the retrograde tracer Fast Blue (FB) (Fig. 3a). Quantification

27   of FB⁺ cells in serial sections of L3 and L4 DRGs, showed that this approach labelled

28   a total of ~340 DRG neurons (191.5 ± 39.8 cells in L3 DRGs and 150.3 ± 56.7 cells in

29   L4 DRGs, Fig. 3a). IB4-labelling of DRG cultures from FB-injected mice, further

30   showed that 35.1% (108/308 FB⁺ cells) of the FB⁺ cells were CHRNA3-EGFP⁺, 25.3

31   % (78/308 FB⁺ cells) were small diameter (<30 μm) IB4⁻ peptidergic nociceptors and

32   26 % (80/308 FB⁺ cells) were large diameter neurons (Fig. 3b) that most likely give rise

33   to group II articular afferents that detect innocuous stimuli. Only a small proportion of

34   the retrogradely labeled neurons were IB4⁺ (13.6%, Fig. 3b), demonstrating that the

6

1 great majority of nociceptive knee joint afferents are peptidergic (IB4⁻ and CHRNA3-

2 EGFP⁺) and that CHRNA3-EGFP⁺ neurons account for ~47 % (108/228 FB⁺

3 nociceptors) of all articular nociceptive afferents. A comparison of the TMEM100

4 expression levels in small diameter (<30 µm) IB4⁻/FB⁺ and CHRNA3-EGFP⁺/FB⁺ cells

5 from the ipsi- and contralateral L3 and L4 DRGs showed that, similar to *in-vitro* NGF

6 treatment, CFA-induced knee joint inflammation selectively up-regulates TMEM100 in

7 CHRNA3-EGFP⁺ MIAs but not in other C-fiber nociceptors (Fig. 3c).

8 We next asked if mechanosensitivity of FB-labelled DRG neurons is altered in CFA-

9 induced monoarthritis. In accordance with our previous results [19], CHRNA3-

10 EGFP⁺/FB⁺ neurons from saline injected animals did not show currents in response to

11 mechanical stimulation of the plasma membrane (Fig. 3d, e). Following intraarticular

12 CFA-injection (3 dpi), however, FB-labelled CHRNA3-EGFP⁺ neurons exhibited robust

13 mechanotransduction currents that were significantly larger than the small inward

14 currents occasionally observed in control animals (Fig. 3d, e). Interestingly, the

15 amplitudes of the mechanotransduction currents of small-diameter IB4⁻ nociceptors

16 were not altered in CFA-treated mice (Fig. 3f), but we observed a small, yet significant,

17 increase in the inactivation time constants of these currents (Fig. 3g). Since TMEM100

18 was previously shown to potentiate the activity of TRPA1 [28], we also examined the

19 responsiveness of FB-labelled neurons to the TRPA1 agonist allylisothiocyanate

20 (AITC) using Calbryte-590 Ca²⁺-imaging. Strikingly, both the amplitude of the AITC-

21 evoked calcium transients as well as the proportion of cells that respond to AITC, were

22 significantly increased amongst MIAs from CFA-treated mice (Fig. 3h), but were

23 completely unaffected in small diameter IB4⁻ nociceptors (Fig. 3i).

24 Taken together, our data showed that intraarticular CFA-injection causes knee joint

25 pain and secondary hyperalgesia in the ipsilateral hind paw, which is accompanied by

26 an upregulation of TMEM100, the potentiation of TRPA1 activity and, most importantly,

27 the acquisition of mechanosensitivity in CHRNA3-EGFP⁺ neurons.

28

29 **TMEM100 knock-out mice develop normal inflammatory knee joint pain but no**

30 **long-lasting secondary mechanical allodynia**

31 We next asked if the pain phenotype of CFA-induced knee monoarthritis (Fig. 2f – h)

32 is causally linked to the sensitization of CHRNA3-EGFP⁺ nociceptors and if this

33 sensitization is induced by the upregulation of TMEM100. To this end we generated

34 conditional TMEM100 knock-out mice, hereafter referred to as TMEM100KO mice, by

1 crossing mice that carry a conditional allele for TMEM100 [35] with SNS-Cre mice, in

2 which Cre-recombinase expression is driven by the voltage-gated sodium channel

3 $Na_v 1.8$ promoter [36] and is thus expressed in all nociceptors including CHRNA3-EGFP[+]

4 neurons [37]. We first compared primary knee joint pain, assessed by gait analysis, in

5 male wildtype (WT) mice that received intraarticular saline injections with male WT and

6 TMEM100KO mice that received CFA injections, over a period of 21 days. WT mice

7 that received CFA, exhibited significantly altered gait, indicative of knee joint pain,

8 during the first seven days post CFA injection compared to saline treated animals.

9 Surprisingly, CFA-treated TMEM100KO mice also developed knee joint pain and

10 showed altered gait (Supplementary movie S3), which significantly differed from saline-

11 treated WT mice (Supplementary movie S1) and was indistinguishable from gait

12 observed in CFA-treated WT mice (Supplementary movie S2; Fig. 4a). Strikingly,

13 however, mechanical allodynia in the ipsilateral hind paw was significantly attenuated

14 in TMEM100KO mice. Thus, the mechanical paw withdrawal thresholds were only

15 transiently reduced from day 3 until day 5 and returned to baseline values by day 7 in

16 TMEM100KO mice, while WT mice exhibited long-lasting secondary mechanical

17 allodynia, which persisted until the end of the examination period (21 dpi, Fig. 4b).

18 Secondary thermal hypersensitivity was not altered in TMEM100KO mice (Fig. 4c).

19 Since an increasing body of literature demonstrates sex differences with regards to

20 pain sensitivity, we reproduced the behavioral experiments using female TMEM100KO

21 mice. Interestingly, female mice exhibited the exact same pain phenotype as male

22 mice with respect to primary and secondary hypersensitivity (Supplementary Fig. 2)

23 indicating a sex-independent role of TMEM100 in inflammatory pain.

24

25 **CFA-induced knee joint inflammation fails to sensitize CHRNA3-EGFP^{+} neurons**

26 **to mechanical stimuli in TMEM100 knock-out mice**

27 We next examined the role of TMEM100 in the acquisition of mechanosensitivity and

28 the potentiation of TRPA1 activity in CHRNA3-EGFP[+] knee joint afferents in CFA-

29 induced monoarthritis. Patch-clamp recordings showed that articular MIAs, (FB-

30 labelled CHRNA3-EGFP^{+} neurons) from TMEM100KO mice did not acquire

31 mechanosensitivity during CFA-induced inflammation (Fig. 5a, b) and that

32 mechanosensitivity of FB[+]/IB^{−} neurons was also not altered (Fig. 5a – d). Moreover, in

33 accordance with the previously described interaction between TMEM100 and TRPA1

34 [28], AITC-induced TRPA1-mediated Ca^{2+}-signals were not potentiated in CHRNA3-

1 EGFP⁺ knee joint afferents from TMEM100KO mice (Fig. 5e), nor were the TRPA1

2 responses of small diameter IB4⁻ nociceptors altered (Fig. 5f).

3 Hence, our data indicates that the un-silencing of silent nociceptors – i.e. the

4 acquisition of mechanosensitivity and the potentiation of TRPA1 – strictly depends on

5 the up-regulation of TMEM100 expression. Considering that secondary mechanical

6 allodynia in the hind paw, but not knee joint pain, was greatly attenuated in

7 TMEM100KO mice during CFA-induced knee inflammation (Fig. 4), together with the

8 observation that the lack of TMEM100 solely altered mechanosensitivity and TRPA1

9 function in CHRNA3-EGFP⁺ afferents, but not in IB4⁻ peptidergic knee joint afferents

10 (Fig. 3 and Fig. 5), we hypothesized that the un-silencing of silent nociceptors triggers

11 the development of secondary mechanical allodynia.

12

13 **Sensitization of cutaneous C-fiber nociceptors contributes to secondary**

14 **mechanical allodynia.**

15 It is well established that secondary mechanical allodynia results from central

16 sensitization – i.e. a strengthening of synaptic transmission in pain processing circuits

17 in the spinal cord [38,39]. Considering the remarkable reduction of paw withdrawal

18 thresholds in CFA-induced knee joint monoarthritis (Fig. 4b), however, we asked if

19 sensitization of cutaneous nociceptors also contributes to secondary mechanical

20 allodynia. To examine peripheral sensitization, we directly measured the

21 mechanosensitivity of C-fiber and Aδ-fiber nociceptors in the tibial nerve, which

22 innervates the plantar surface of the hind paw, by recording mechanically evoked

23 action potentials from single nerve fibers in an ex-vivo skin-nerve preparation from

24 mice that had received intraarticular CFA (Fig. 6a, b and Supplementary Fig. 3). These

25 recordings revealed, that 40% of the cutaneous C-fiber nociceptors from mice with

26 CFA-induced knee monoarthritis, are activated by forces of 0.16 g and below and

27 virtually all C-fibers (90%) responded to von Frey filaments of 0.4 g and below (Fig. 6a

28 – d). By contrast, not a single C-fiber nociceptor from saline-treated control mice

29 responded to von Frey stimuli ≤ 0.16g and only ~17% were activated by the 0.4 g

30 filament (Fig. 6a – d). Moreover, cutaneous C-fibers from CFA-treated mice also fired

31 significantly more action potentials in response to suprathreshold mechanical ramp-

32 and-hold stimuli applied with a piezoelectric micromanipulator (Fig. 6e). Aδ-fiber

33 nociceptors also showed a trend towards being more sensitive, but this difference was

34 less pronounced than in C-fibers (Supplementary Fig. 3b). Likewise, the firing rate was

1 slightly higher in Aδ-fiber nociceptors from CFA-treated mice, but only significant for

2 the largest tested suprathreshold stimulus (Supplementary Fig. 3c). Strikingly, the

3 mechanical activation thresholds and the firing rates of both C-fiber nociceptors and

4 Aδ-fiber nociceptors from CFA-treated TMEM100KO mice were indistinguishable from

5 those of saline-treated WT control mice (Fig. 6d, e and Supplementary Fig. 3b and c).

6 Taken together, these results show that CFA-induced knee joint inflammation shifts

7 the mechanosensitivity of individual cutaneous C-fiber nociceptors towards innocuous

8 mechanical stimuli, which correlates with the leftward shift of the paw withdrawal

9 thresholds in the same mice. Hence, our data suggests that in addition to central

10 sensitization, sensitization of cutaneous C-fiber and Aδ-fiber nociceptors might also

11 significantly contribute to secondary mechanical allodynia in the hind paw induced by

12 knee joint inflammation.

13

14 **Overexpression of TMEM100 in articular afferents induces secondary allodynia**

15 **in the hind paw but no knee joint pain.**

16 While the spinal and supraspinal mechanisms of central sensitization that underlie

17 secondary hyperalgesia are well understood, only little is known about the initial signals

18 that trigger the development of secondary allodynia [38,40]. Considering that inhibition of

19 un-silencing of MIAs by knocking out TMEM100 prevents the development of long-

20 lasting secondary allodynia, our data suggests that MIAs might be essential for the

21 induction of secondary allodynia. To test this hypothesis, we next un-silenced articular

22 MIAs without inducing an inflammation. To this end, we selectively overexpressed

23 TMEM100 in knee joint afferents by intra-articular injection of an AAV-PHP.S-

24 TMEM100-Ires-dsRed virus (30 µl, $1.5*10^{11}$ vg; Fig. 7a). Four days after intraarticular

25 AAV-PHP.S-TMEM100-Ires-dsRed administration, we observed prominent dsRed

26 fluorescence in a total of 339 ± 7 neurons in ipsilateral L3 and L4 DRG (Fig. 7a). Most

27 importantly, we observed numerous dsRed expressing nerve fibers in the saphenous

28 nerve proximal to the knee (Fig. 7b), which includes the medial articular nerve that

29 supplies the knee joint and in which silent nociceptors had first been described [11], but

30 hardly any dsRed⁺ fibers in the tibial nerve distal to the knee, which contains cutaneous

31 afferents that supply the plantar surface of the hind paw (Fig. 7b). Hence,

32 intraarticularly administered AAV-PHP.S-TMEM100-Ires-dsRed causes selective

33 overexpression of TMEM100 in knee joint afferents, but not in afferents that supply the

34 plantar surface of the hind paw. Interestingly, TMEM100-overexpressing mice

1 exhibited normal gait, indicating that un-silencing of knee joint MIAs does not trigger

2 knee joint pain (Fig. 7c). Strikingly, however, these mice developed profound

3 mechanical hypersensitivity in the ipsilateral hind paw five days post AAV injection,

4 which persisted until the end of the observation period (21 dpi; Fig. 7d). Thus, the

5 mechanical paw withdrawal thresholds decreased from 0.92 ± 0.066 g (-1 dpi) to 0.373

6 ± 0.035 g (14 dpi). Mice that received a control virus without TMEM100 (AAV-PHP.S-

7 dsRed) did not show any signs of mechanical hypersensitivity. In accordance with the

8 behavioral outcome of TMEM100 over-expression in articular afferents, single-unit

9 action potential recordings from a tibial nerve-glabrous skin preparation showed that

10 cutaneous C-fiber nociceptors fire about twice as many action potentials in response

11 to a given stimulus and have significantly reduced mechanical activation thresholds in

12 mice that overexpress TMEM100 in articular afferents compared to mice that had

13 received a control virus (Fig. 7e – g). Similar to mice that received intraarticular CFA,

14 the mechanical activation thresholds of cutaneous Aδ-fiber nociceptors were slightly

15 reduced and the action potential firing rate in response to suprathreshold stimuli was

16 significantly increased (Supplementary Fig. 4).

17 In summary, our data shows that TMEM100 overexpression-induced un-silencing of

18 mechanically insensitive articular afferents is sufficient to trigger mechanical

19 hypersensitivity in remote skin regions (Fig. 7d). Together with the observation that

20 TMEM100 is specifically up-regulated in MIAs during CFA-induced inflammation and

21 that knock-out of TMEM100 exclusively abolishes long-lasting secondary allodynia,

22 these results suggest that sensory input from unsilenced MIAs is the main trigger for

23 the induction of secondary allodynia (Fig. 7h). While we have not examined the well-

24 established contribution of central sensitization, our data reveals a previously

25 unrecognized contribution of peripheral sensitization to secondary allodynia.

26

Discussion

28 The peculiar properties of MIAs have fueled speculations about a prominent

29 contribution to inflammatory pain ever since they had first been described more than

30 thirty years ago [11,17,41], but hitherto, neither the molecular mechanism underlying their

31 un-silencing, nor their exact role in pain signaling have been deciphered.

32 We have previously shown that *in-vitro* NGF-induced un-silencing of MIAs requires *de-*

33 *novo* gene transcription and that mechanosensitivity in MIAs is mediated by the

34 mechanically-gated ion channel PIEZO2, the expression of which is, however, not

1   changed during un-silencing (Fig. 1d) [19]. Here we show that TMEM100 is specifically

2   up-regulated in CHRNA3-EGFP+ MIAs during inflammation (Fig. 1d, e and Fig. 3c) and

3   demonstrate that over-expression of TMEM100 is sufficient to un-silence MIAs *in-vitro*

4   (Fig. 1f – h), whereas knock-out of TMEM100 prevents un-silencing in a mouse model

5   of CFA-induced monoarthritis (Fig. 5b, d). Considering that CHRNA3-EGFP+ MIAs

6   express high levels of PIEZO2 even in conditions in which they are not

7   mechanosensitive [19] (Fig. 1d) and that PIEZO2 does not require the presence of an

8   auxiliary subunit for normal function, we hypothesize that PIEZO2 is somehow kept

9   'silent' in these neurons under normal conditions and is primed by the up-regulation of

10   TMEM100. CHRNA3-EGFP+ MIAs express four known PIEZO2 inhibitors, namely

11   MTMR2 [22], SERCA2 (Atp2a2) [26], Annexin A6 (Anxa6) [25] and Nedd4-2 [27], but since

12   neither of them is down-regulated by NGF (Fig. 1sd) and all four are ubiquitously

13   expressed in sensory neurons [2], it seems highly unlikely that any of them is involved

14   in keeping PIEZO2 silent in MIAs. Hence, while our study identified TMEM100 as a

15   key protein that is sufficient and required for the un-silencing of MIAs, the mechanism

16   by which PIEZO2 is kept inactive in CHRNA3-EGFP+ MIAs remains elusive.

17   TMEM100 had originally attracted our attention because it was previously shown to

18   enhance TRPA1 activity in a TRPV1-dependent manner [28] and because there is ample

19   evidence supporting a role of TRPA1 in fine-tuning mechanosensitivity of sensory

20   afferents. Thus, it was shown that pharmacological blockade as well as knock-out of

21   TRPA1 partially inhibit mechanotransduction currents in cultured DRG neurons and

22   reduce the firing rate of cutaneous C-fiber nociceptors [42–45]. Since TRPA1, to the best

23   of our knowledge, is not activated by mechanical indentation of the cell membrane but

24   is directly gated by intracellular calcium [46], a possible mechanistic explanation for the

25   role of TRPA1 is that it increases mechanosensitivity of sensory neurons by amplifying

26   PIEZO2-mediated Ca^{2+} influx. Consistent with the findings of Weng and colleagues [28],

27   we found that CFA-induced knee joint inflammation enhances TRPA1 activity in a

28   TMEM100-dependent manner (Fig. 3h and Fig. 5e). Most importantly, our data

29   substantiate and extend the findings of Weng et al. (2015), by showing that TMEM100

30   is exclusively up-regulated in CHRNA3-EGFP+ neurons – at least in CFA-induced knee

31   monoarthritis and after in-vitro NGF treatment (Fig. 1d, e and Fig. 3c) – and accordingly

32   only enhances TRPA1 activity in MIAs but not in other nociceptors (Fig. 3h, i and Fig.

33   5e, f).

12

1   Hence our data suggests that TMEM100 is a pleiotropic protein that on the one hand

2   induces mechanosensitivity in MIAs by priming PIEZO2 via a yet unknown mechanism

3   and on the other hand amplifies PIEZO2-dependent mechanosensitivity by releasing

4   TRPA1 from inhibition by TRPV1.

5

6   Primary hyperalgesia has an adaptive role as it produces behaviors that promote

7   healing and recovery. It results from peripheral sensitization – i.e. direct sensitization

8   of nerve endings in the inflamed or injured tissue – and usually resolves concurrently

9   with the initial cause of pain. Secondary allodynia and hyperalgesia, on the other hand,

10 are considered maladaptive and result from central sensitization – i.e. a strengthening

11 of synaptic transmission in pain processing circuits in the spinal cord [38–40]. Moreover,

12 secondary allodynia is thought to increases the likelihood of developing chronic pain

13 as, for example, the area and intensity of secondary allodynia immediately after

14 surgery correlates with the incidence of persistent postsurgical pain [47].

15 While the spinal mechanisms of central sensitization have been studied extensively in

16 various rodent pain models, including experimentally induced arthritis [48–50], the

17 peripheral inputs that initially trigger the development of central sensitization and hence

18 secondary allodynia are still unknown. Here we show that blocking the un-silencing of

19 articular MIAs by knocking out TMEM100 prevents the development of long-lasting

20 secondary allodynia in remote skin regions, but does not alter pain at the actual site of

21 CFA-induced inflammation (Fig. 4). Moreover, TMEM100 overexpression-induced un-

22 silencing of knee joint MIAs in the absence of inflammation or injury, induces

23 mechanical hypersensitivity in the paw but not pain hypersensitivity in the knee joint

24 (Fig. 7c, d). Finally, our skin-nerve recordings demonstrate that secondary allodynia,

25 in addition to the previously described central sensitization, is partly driven by

26 peripheral sensitization of cutaneous C-fiber nociceptors (Fig. 6 and Fig. 7e – g).

27 Regarding the AAV-mediated TMEM100 over-expression experiments, one should

28 note that intra-articularly administered AAV-PHP.S infects all subclasses of sensory

29 afferents in the knee joint and thus the observed secondary allodynia could

30 theoretically also result from TMEM100 over-expression in articular afferents other

31 than CHRNA3-EGFP⁺ MIAs. Although we cannot completely rule out this possibility, a

32 contribution of other nociceptor subtypes to the induction of secondary allodynia seems

33 unlikely, because if ectopic TMEM100 overexpression had also increased the activity

34 other nociceptors in the knee joint, then we should have observed knee joint pain – i.e.

1 changes in gait – in addition to secondary allodynia, which was, however, not the case

2 (Fig. 7c). Moreover, the observation that TMEM100 expression is exclusively

3 upregulated in MIAs in CFA-induced monoarthritis (Fig. 3c) and that mice lacking

4 TMEM100 only show functional deficits in MIAs but not in other articular nociceptors

5 (Fig.3 and 5) and selectively lose secondary allodynia but not knee joint pain, strongly

6 support a specific role of MIAs in inducing secondary allodynia. It should further be

7 noted, that we observed off-target expression of TMEM100 in a few fibers in the tibial

8 nerve distal to the knee, which supplies the plantar surface of the hind paw (Fig. 7b).

9 Cutaneous C-fiber nociceptors that detect von Frey stimuli express MRGPRD [7] and

10 require PIEZO2 and TRPA1 for normal mechanosensitivity [43,52], but do not express

11 TRPV1 [2,7]. Since TMEM100, however, only sensitizes PIEZO2 in the specific cellular

12 environment of CHRNA3-EGFP[+] MIAs (Fig. 1f – h and Supplementary Fig. 1) and

13 enhances TRPA1 in a TRPV1-dependent manner – in fact it inhibits TRPA1 in the

14 absence of TRPV1 [28] – the off-target expression of TMEM100 in a few cutaneous nerve

15 fibers most likely does not contribute to the observed secondary hyperalgesia in the

16 hind paw.

17 We have not explicitly tested if un-silencing of MIAs also triggers central sensitization,

18 which is thought to be the major cause of secondary hypersensitivity. Yet, considering

19 that the AAV-PHP.S-TMEM100 induced reduction of paw withdrawal thresholds (Fig.

20 7d) was larger than the reduction of the mechanical activation thresholds of individual

21 cutaneous C- and Aδ-fiber nociceptors (Fig. 7g and Fig 4c), it seems highly likely that

22 central processing of nociceptive input was also altered in these experiments such that

23 subliminal sensory inputs evoked pain.

24 Hence, our data support a mechanistic model of secondary allodynia in which

25 inflammation-induced upregulation of TMEM100 un-silences MIAs, which

26 subsequently triggers central sensitization and – via a yet unknown central mechanism

27 – peripheral sensitization of cutaneous nociceptors, which eventually leads to

28 secondary mechanical allodynia in skin regions remote from the site of inflammation

29 (Fig. 7h). By demonstrating that primary and secondary pain hypersensitivity are

30 triggered by separate subclasses of primary sensory afferents and considering that

31 MIAs constitute almost fifty percent of all nociceptors in viscera and deep somatic

32 tissues, our study provides an invaluable framework for future studies that aim at

33 deciphering the contribution of different afferent subtypes to other clinically relevant

1 forms of pain and to develop new strategies for preventing the transition from acute to

2 chronic of pain after injury, inflammation or surgical interventions.

3

Methods

Animals

6 All experiments were conducted in accordance with the European Communities

7 Council Directive (EU and institutional guidelines) including the ethical guidelines of

8 'Protection of Animals Act' under supervision of the 'Animal Welfare Officers' of

9 Heidelberg University and were approved by the local governing body

10 (Regierungspraesidium Karlsruhe, approval number G16/20). ARRIVE guidelines

11 were followed and sample sizes were calculated as previous experience with G-power

12 analyses.

13 CHRNA3-EGFP mice (Tg(Chrna3-EGFP)BZ135Gsat/Mmnc) were purchased from the

14 Mutant Mouse Resource & Research Center (MMRRC) and were backcrossed to a

15 C57Bl/6J background. Conditional nociceptor TMEM100 knock-out mice were

16 generated by crossing mice that carry a conditional allele for TMEM100

17 (B6.Tmem100tm1.1Yjl) [35] with SNS-Cre mice C57BL/6-Tg(SCN10A-Cre)1Rkun/Uhg

18 [36] (gift from Rohini Kuner). To enable identification of MIAs, these mice were further

19 crossed with CHRNA3-EGFP mice. Furthermore, to identify different nociceptor

20 subclasses for RT-qPCR experiments, Tg(Npy2r-cre)SM19Gsat/Mmucd x B6;129S-

21 Gt(ROSA)26Sortm32(CAG-COP4*H134R/EYFP)Hze/J   (Npy2rCre;ChR2-EYFP)

22 mice, in which Aδ-fiber nociceptors express EYFP were used [6]. Mice were maintained

23 in the Interfaculty Biomedical Facility of Heidelberg University according to institutional

24 guidelines on a 12/12-hour light-dark cycle in an enriched housing environment and

25 had access to food and water ad libitum. For all experiments only adult (age 8-15

26 weeks) male and female mice were used. Behavioral experiments were conducted at

27 the Interdisciplinary Neurobehavioral Core of Heidelberg University. Prior to the start

28 of experiments animals with the same genetic background and age were randomly

29 assigned to the different experimental groups. To reduce bias investigators were

30 blinded to group identity including treatment (CFA/Saline) and genotype

31 (TMEM100KO/WT).

32

HEK293 cell maintenance and transfection

15

1 To assess the mechanosensitivity of TMEM100 and of PIEZO2 in the presence and

2 absence of TMEM100, the constructs were (co)-transfected into HEK293 cells using

3 the calcium phosphate method. Cells were grown in DMEM (Thermo Fisher)

4 supplemented with 10% FBS (Thermo Fisher), 2 mM L-glutamine (Thermo Fisher) and

5 penicillin streptomycin (Thermo Fisher, 100 U/mL) at 37ºC and 5% CO_2. The day

6 before transfection, cells were seeded on poly-L-lysine treated glass coverslips. For

7 transfection, growth medium was replaced with transfection medium consisting of

8 DMEM, 10% calf serum (Thermo Fisher) and 4 mM L-Glutamine. DNA (0.6

9 µg/coverslip) was diluted in 100 µl water and after adding $CaCl_2$ 2.5M (10 µL per

10 coverslips) the solution was vigorously mixed. Then, 2 x BBS (in mM, 50 HEPES, 280

11 NaCl, 1.5 Na_2HPO_4, pH 7.0; 100 µL/coverslip) was added and vortexed. The resulting

12 DNA mix was added to the transfection medium. After 3-4 hours at 37ºC (5% CO_2) the

13 transfection medium/DNA mix was replaced with regular HEK293 growth medium.

14 PIEZO2 function was assessed 48 h after transfection.

15

16 **Primary DRG cell culture**

17 For primary DRG cultures, mice were sacrificed by placing them in a CO_2-filled

18 chamber for 2–4 min followed by cervical dislocation. Lumbar L3 and L4 DRG were

19 collected in Ca^{2+} and Mg^{2+}-free PBS. DRG were subsequently treated with

20 collagenase IV for 30 minutes (0.5 mg/ml, Sigma-Aldrich, C5138) and with trypsin (0.5

21 mg/ml, Sigma-Aldrich, T1005) for further 30 minutes, at 37 °C. Digested DRG were

22 washed twice with growth medium [DMEM-F12 (Gibco®, Thermo Fisher Scientific)

23 supplemented with L-glutamine (2 µM, Sigma-Aldrich), glucose (8 mg/ml, Sigma-

24 Aldrich), penicillin (200 U/ml)–streptomycin (200 µg/ml) (Gibco®, Thermo Fisher

25 Scientific), 5 % fetal horse serum (Gibco®, Thermo Fischer Scientific)], triturated using

26 a pipette with filter tips of decreasing diameter (10x up and down with 1000µl filter tip,

27 10x up and down with 200µl filter tip) and plated in a droplet of growth medium on a

28 glass coverslip precoated with Laminin (GG-12-Laminin coated coverslips, Neuvitro).

29 To allow the dissociated neurons to adhere, coverslips were incubated for 3 hours at

30 37 °C in a humidified 5 % incubator before being flooded with fresh growth medium.

31 Depending on the experiment neurons were used directly after adding fresh growth

32 medium (see Reverse transcription and quantitative real-time PCR) or after 24h of

33 incubation (see Patch-clamp recordings). For the experiments shown in Fig. 1f – h,

1   primary DRG cultures were transfected using the Amaxa Nucleofector 4D (Lonza)

2   following the manufactures instructions.

3

4   **Inflammatory knee pain model**

5   To induce inflammatory knee joint pain the Complete Freund's Adjuvant (CFA)-induced

6   knee joint monoarthritis model was used as previously described [53]. In brief, animals

7   were anesthetized in a transparent plexiglass chamber filled with 4% isoflurane in

8   100% O2 at a flow rate of 1.0 L/min for 3 min. During the procedure anesthesia was

9   maintained using a nosecone delivering a 1.5% Isofluran-O2 mixture while respiratory

10 function was monitored carefully. Adequate anesthesia was confirmed by absence of

11 the pedal reflex (toe pinch). Then, ophthalmic ointment was applied to both eyes to

12 prevent desiccation and the animals were placed in a supine position. Prior to injection

13 of CFA, the left knee was shaved using a commercially available electrical facial hair

14 trimmer, disinfected with povidone-iodine scrub (7.5% solution, Braunol®) and

15 stabilized in a bent position by placing the index finger beneath the knee joint and the

16 thumb above the anterior surface of the ankle joint. The patellar tendon shining through

17 the shaved skin served as visual landmark for the injection. To ensure a precise

18 intraarticular (i.a.) injection the gap inferior to the lower edge of the patella was

19 identified by running a 30 G Insulin syringe horizontally along the knee. To mark the

20 injection level gentle pressure was applied to skin without piercing it leaving behind a

21 horizontal dermal print line. For the injection the needle was lifted vertically at the

22 marked level and inserted at the midline through the patella tendon perpendicular to

23 the tibial axis. Then, the needle was advanced approximately 2-2.5mm without

24 resistance to fully enter the knee joint and 30µl of CFA (1µg/µl) or saline were injected

25 into the joint cavity. After the procedure, the injection site was disinfected and the knee

26 was briefly massaged and mobilized to ensure even distribution of CFA/saline before

27 the animals were returned to their home cages placed on a heating pad for recovery.

28

29 **Behavioral testing**

30 All behavioral tests were performed in awake, unrestrained mice by experienced

31 investigators blinded to group identity. Before testing, all animals were habituated to

32 the behavioral test setups at least 3 times over a total of 3 days (1x/d per setup) in the

33 week before starting the behavioral experiment. For the von Frey (vF) and Hargreaves'

34 test animals were habituated for 1h/setup, and 30 to 60 minutes immediately before

17

1   each test with the experimenter present in the same room. For the CatWalk XT a

2   habituation session was completed when mice voluntarily crossed the runway 3 times

3   without stopping, turning around, or changing direction (approx. 5 min/animal). On

4   testing days, acclimatization to the CatWalk setup was not necessary. Behavioral

5   assays were always carried out in the same order (CatWalk, vF, Hargreaves) using

6   the same rooms and same test setups at the same time point of the day between 8

7   a.m - 3 p.m. Prior to knee injection, at least two baseline measurements on two

8   different days were conducted for all behavioral tests. After injections, behavior was

9   evaluated 1, 2, 3, 5 and 7 days post injection (dpi) and then in weekly intervals (14 dpi)

10 for a total of 3 weeks (21dpi).

11

12 **Von Frey Test: mechanical sensitivity**

13 Mechanical sensitivity was assessed using the von Frey test as described previously

14 [54] 3. Animals were placed in transparent plastic chambers (Modular animal-enclosure;

15 Ugo Basile Srl, Gemonio, Italy) on a 90x38 cm perforated metal shelf (Framed testing

16 surface; Ugo Basile Srl, Gemonio, Italy) that was mounted on a stimulation base. The

17 plantar surface of the animals' hind paws was perpendicularly stimulated with graded

18 von Frey filaments (Aesthesio® Precision Tactile Sensory Evaluators) of different

19 forces, ranging from 0.07 to 1.4 g without moving the filaments horizontally during

20 application. Each filament was applied 5 times to both the right and left hind paws and

21 the response rate to stimulation in percent (positive response/number of applied

22 stimuli) was used to express mechanical sensitivity. Withdrawal of the stimulated paw

23 was defined as a positive response. Between stimulations of the same hind paw

24 animals had least 1 min break. Prior to knee injection baseline withdrawal frequencies

25 were determined by measuring the withdrawal response rates for all filaments on two

26 different days. After injections, mechanical sensitivity was evaluated 1, 2, 3, 5 and 7

27 days post injection (dpi) and then in weekly intervals for a total of 3 weeks (21dpi). The

28 50% withdrawal threshold (WDT) in grams was determined by fitting the response rate

29 vs. von Frey force curves with a Boltzmann sigmoid equation with constant bottom and

30 top constraints equal to 0 and 100, respectively.

31

32 **Hargreaves' test: thermal sensitivity**

33 Thermal sensitivity was assessed according to Hargreaves' method [55] using the

34 Plantar test (Hargreaves Apparatus; Ugo Basile Srl). In brief, withdrawal latency (WDL)

18

1   in seconds to an infrared (IR) heat beam stimulus applied to the plantar surface of the

2   hind paws was recorded to determine thermal sensitivity. The IR intensity of the radiant

3   heat source was adjusted to obtain baseline WDL between 5 and 7 seconds (IR

4   intensity 50%), with a pre-determined cut-off time of 15 seconds to prevent tissue

5   damage. Each paw was assessed three times and between trials for the same paw,

6   animals had at least an one minute break. To prevent an order effect the paw testing

7   order was chosen randomly. Baseline and post-interventional measurements were

8   conducted at the same time points as described for the vF test.

9

10 **CatWalk XT: gait analysis**

11 To quantitatively assess locomotion, the CatWalk XT (version 10.6) gait analysis

12 system (Noldus, Netherlands system) was used. This system consists of an enclosed

13 black corridor (1.3m length) on a glass plate. Inside this glass plate a green LED light

14 is internally reflected. When animals touch the glass plate the light is refracted on the

15 opposite side so that areas of contact become illuminated and detectable. Using the

16 Illuminated Footprints™ technology, videos including the illuminated areas (e.g. paw

17 prints) can be recorded using a high speed color camera (100 frames/s) that is

18 positioned underneath the glass plate. The data is automatically transferred to

19 computer running the CatWalk XT software for further gait analysis. Animals were

20 habituated to the set up as described above (see Behavioral testing). On testing days,

21 animals were placed on one end of the corridor and were allowed to transverse it

22 voluntarily without any external enforcement after setting up the walkway according to

23 the manufacturer's recommendations. For each mouse on each measurement time

24 point three compliant runs were recorded. A compliant run was defined as a mouse

25 walking across the runway without stopping, turning around, or changing direction and

26 meeting the following pre-determined run criteria: minimum run duration of 0.5s and a

27 maximum run duration of 12s. For all runs the same detection settings were used

28 (camera gain: 16.99, green intensity threshold: 0.10, red ceiling light: 17.7, green

29 walkway light: 16.5). In our analyses we focused on the following gait parameters:

30 stand time in seconds, paw print area in cm^2, swing speed in cm/s. To better illustrate

31 pain-associated changes in the gait cycle including the stand and swing phase, run

32 data of the left (LH) and right hind paw (RH) are displayed as ratio (LH/RH). For each

33 testing day the ratios (LH/RH) of all three runs per animal were averaged so that the

1   mean of three compliant runs represents the overall result of the animal on that testing

2   day.

3

Retrograde labeling

5   To identify sensory neurons innervating the knee joint retrograde labeling with Fast

6   Blue (FB, #17740-1, Polysciences) was performed. To this end, the same

7   anesthesiological and surgical approach was used as described above (see

8   Inflammatory knee pain model). 2µl of a 4% FB (in saline) solution were injected i.a. in

9   both knee joints using a 10µl Hamilton syringe fitted with 30G needle. After a waiting

10   period of 7d allowing the FB to retrogradely travel to the DRG, animals were further

11   processed depending on the following experiment. To quantify the knee innervating

12   neurons (Fig 3a), animals were sacrificed for microscopy (see Tissue processing and

13   immunochemistry). For electrophysiological and qPCR experiments, the left knee was

14   injected again, but with CFA as described above (see Inflammatory knee pain model)

15   and 3 days thereafter – at the time of maximum pain – the animals were euthanized

16   for primary DRG cultures.

17

Patch-clamp recordings

19   Whole cell patch clamp recordings were made from retrogradely FB-labelled sensory

20   neurons innervating the knee (see Retrograde labeling). To distinguish between MIAs

21   and other peptidergic nociceptors, CHRNA3-EGFP$^+$/FB$^+$ neurons and small (<30µm)

22   IB4$^-$/FB$^+$ neurons (see Immunohistochemistry) were recorded, respectively. These two

23   subpopulations account for the majority of nociceptive knee joint afferents (see Fig.

24   3b). Cells from both WT and TMEM100KO animals after CFA and control treatment

25   were assessed. To this end, 7d after retrograde labeling of the DRG from both knees

26   animals received a second injection into the left knee using CFA or Saline. 3d after this

27   second injection, at the time of maximum CFA-induced pain behavior, the animals

28   were sacrificed. L3 and L4 DRG from the ipsi- (CFA/Saline) and contralateral side were

29   collected separately and cultured for 16-24h (see Primary DRG culture) until used for

30   whole cell patch clamp recordings.

31   Whole cell patch clamp recordings were made at room temperature (20-24°C) using

32   patch pipettes with a tip resistance of 2-4 MΩ that were pulled (Flaming-Brown puller,

33   Sutter Instruments, Novato, CA, USA) from borosilicate glass capillaries (BF150-86-

34   10, Sutter Instrument). The patch pipettes were filled with a solution consisting of 110

1   mM KCl, 10 mM NaCl, 1 mM $MgCl_2$, 1 mM EGTA, 10 mM HEPES, 2 mM guanosine

2   5'-triphosphate (GTP) and 2 mM adenosine 5'-triphosphate (ATP) adjusted to pH 7.3

3   with KOH. The bathing solution contained 140 mM NaCl, 4 mM KCl, 2 mM CaCl2, 1

4   mM $MgCl_2$, 4 mM glucose, 10 mM HEPES and was adjusted to pH 7.4 with NaOH. All

5   recordings were made using an EPC-10 amplifier (HEKA, Lambrecht, Germany) in

6   combination with Patchmaster© and Fitmaster© software (HEKA). Pipette and

7   membrane capacitance were compensated using the auto function of Patchmaster and

8   series resistance was compensated by 70 % to minimize voltage errors. Mechanically

9   activated currents were recorded in the whole-cell patch-clamp configuration. Neurons

10   were clamped to a holding potential of -60 mV and stimulated with a series of

11   mechanical stimuli in 0.8 µm increments with a fire-polished glass pipette (tip diameter

12   2-3µm) that was positioned at an angle of 45° to the surface of the dish and moved

13   with a velocity of 3 µm/ms by a piezo based micromanipulator called nanomotor©

14   (MM3A, Kleindiek Nanotechnik, Reutlingen, Germany). The evoked whole cell currents

15   were recorded with a sampling frequency of 200 kHz. Mechanotransduction current

16   inactivation was fitted with a single exponential function $(C1+C2*\exp(-(t-t0)/\tau_{inact})$,

17   where C1 and C2 are constants, t is time and τ_{inact} is the inactivation time constant [56].

18

19   **Tissue processing and immunochemistry**

20   To quantify retrogradely labelled neurons, DRG were dissected in ice-cooled PBS,

21   fixed with Zamboni´s fixative for 1 h at 4 °C and incubated overnight in 30 % sucrose

22   at 4°C. Then, DRG were embedded in optimum cutting temperature compound

23   (Tissue-Tek™ O.C.T. Compound; Sakura Finetek Germany GmbH, Staufen), cut into

24   16 µm cryo-sections using a cryostat (Leica CM1950, Leica, Wetzlar, Germany) and

25   mounted onto slides (Microscope Slides SUPERFROST PLUS; Thermo Fisher

26   Scientific, Schwerte, Germany) which were stored at -80˚C until used for

27   immunohistochemistry. After drying, sections were treated with 50 mM Glycine in PBS

28   for 20 min, washed twice with 0.2 % Triton X-100 in PBS (0.2% PBST), blocked with

29   10% normal donkey serum (NDS) and 1% bovine serum albumin (BSA) in 0.2% PBST

30   for 30 min and then incubated with primary antibodies overnight at 4°C. Primary

31   antibodies were diluted in the blocking solution (10% NDS and 1% BSA in 0.2% PBST).

32   Next day, sections were washed 4 x 15 min with 0.2% PBST, subsequently incubated

33   with secondary antibodies for 1 h at room temperature (RT), washed with 0.2% PBST

1   four times (15 min each), dried and coverslipped with FluoroGel (FluoProbes®,

2   Interchim, Montluçon France).

3   Cultured DRG neurons (see Primary DRG cultures) for electrophysiological and qPCR

4   experiments were counterstained with Alexa Fluor™ -568 conjugated IB4 (2.5µg/ml,

5   Isolectin GS-IB from Griffonia simplicifolia, Alexa Fluor™ 568 Conjugate,

6   Invitrogen™/Thermo Fischer Scientific, I21412) for 10-15 minutes at room temperature

7   to identify different nociceptor subpopulations (CHRNA3-EGFP$^+$/FB$^+$ and IB4$^-$/FB$^+$

8   neurons).

9   Knees were dissected in cold PBS and fixed with Zambonis fixative overnight. Then,

10 the knee joints were washed in purified water (Milli-Q, Merck KGaA, Darmstadt,

11 Germany) for 3x 30 min before being decalcified by submerging the samples in 10 %

12 EDTA in PBS for 7-10 days (PBS/EDTA was replaced every other day) on a tube roller

13 mixer at 4 °C. After decalcification the samples were washed in PBS for 3 x10 min at

14 RT and cryoprotected in 30% sucrose solution at 4 °C for at least 24h. For the

15 preparation of tissue sections, samples were embedded in optimum cutting

16 temperature compound (Tissue-Tek™ O.C.T. Compound; Sakura Finetek Germany

17 GmbH, Staufen), cut into 25 µm consecutive coronal cryo-sections in arterior-posterior

18 direction and mounted onto microscope slides (SUPERFROST PLUS; Thermo Fisher

19 Scientific, Schwerte, Germany). After drying at RT for 1h, sections were incubated with

20 50 mM Glycine in PBS for 30 min, washed and blocked 3 x 10 min with 0.5% Tween®

21 20 in PBS (0.5% PBS-Tw) and then incubated with primary antibodies for 3d at 4°C.

22 Primary antibodies were diluted in a PBS solution containing 1% BSA and 0.3% Triton

23 X-100. Sections were then washed 3 x 10 min with 0.5% PBS-Tw and subsequently

24 incubated for 2 hours at RT with secondary antibodies diluted in PBS with 1% BSA

25 and 0.3% Triton X-100. Finally, the slides were washed with PBS (3 x 10 min), dried

26 and coverslipped using FluoroGel mounting medium with 4,6-diamidino-2-

27 phenylindole (DAPI) counter stain (FluoProbes®, Interchim, Montluçon FRANCE).

28 Immunostaining images were captured with the Nikon DS-Qi2 camera mounted on a

29 Nikon Ni-E epifluorescence microscope using appropriate filter cubes and identical

30 exposure times for all slides within one experiment.

31 Silent afferent density (EGFP$^+$/CGRP$^+$ fibers) was quantified in anatomical regions

32 including FP (Hoffa's fat pad), LM (lateral meniscus), MM (medial meniscus), LJC

33 (lateral joint capsule), MJC (medial joint capsule) and CL (cruciate ligament) defined

34 according to landmarks as previously described [57] using the area fraction tool of NIH

1   ImageJ software (ImageJ 1.53e; Java 1.8.0_172 [64-bit]). In brief, after conversion to

2   8-bit and background subtraction, image auto local thresholds were set using the

3   Bernsen method. Then, the different immunostaining images (channels) were merged

4   and processed using the image calculator tool to display only double positive

5   (EGFP$^+$/CGRP$^+$) signals. Finally, the predefined anatomical regions of interest were

6   overlaid and the area fraction determined representing the labelling density of silent

7   afferents per anatomical region in percent. For each animal, at least three

8   photomicrographs per anatomical region were analyzed and averaged. The labelling

9   density per anatomical region for all animals was expressed as mean ± SEM. For

10   illustration purposes (Fig. 2a) representative images of coronal 100 μm knee sections

11   (Cryostat) were acquired and stitched using a Leica SP8 Confocal microscopy platform

12   equipped with a Lasx 3.5. Laser, detector powers were optimized for the combination

13   of antibodies.

14

15   **Antibodies**

16   The following primary antibodies were used: rat anti-GFP (Nacalai tesque, #04404-84,

17   1:3000), rabbit anti-CGRP (ImmunoStar,#24112, 1:200), Isolectin GS-IB from Griffonia

18   simplicifolia Alexa Fluor™ 568 Conjugate (2.5μg/ml, Invitrogen™/Thermo Fisher

19   Scientific, #I21412), Isolectin GS-IB from Griffonia simplicifolia Alexa Fluor™ 647

20   Conjugate (2.5μg/ml, Invitrogen™/Thermo Fisher Scientific, #I32450) and rabbit anti-

21   dsRed (1:1000; Takara). The following corresponding Alexa Fluor™ conjugated

22   secondary antibodies (1:750; Thermo Fisher Scientific) were used: Alexa Fluor 488

23   conjugated donkey anti-Rat IgG (Thermo Fisher Scientific,#A48269), Alexa 594

24   conjugated donkey anti-Rabbit IgG (Thermo Fisher Scientific, #A32754).

25

26   **Reverse transcription and quantitative real-time PCR**

27   To compare NGF-induced changes in mRNA expression levels of TMEM100 in

28   different nociceptor subclasses (Fig. 1e), primary L3-4 DRG neurons from WT mice

29   were cultured in the absence and presence of NGF (50 ng/ml) for 24h before cell

30   collection. To compare mRNA expression levels of TMEM100 in treated (CFA) and

31   control (saline) knee innervating nociceptors at the time of maximum pain (3 dpi),

32   CHRNA3-EGFP$^+$/FB$^+$ and IB4$^-$/FB$^+$ neurons from the ipsi- (CFA) and contralateral

33   (saline) side were collected from acute primary L3-4 DRG cultures of WT mice

34   immediately after adding fresh growth medium without further incubation. In both

1 approaches cultures were counterstained with Alexa Fluor™ -568 conjugated IB4

2 (2.5µg/ml, Isolectin GS-IB from Griffonia simplicifolia, Alexa Fluor™ 568 Conjugate,

3 Invitrogen, I21412) for 10-15 minutes at room temperature to enable the identification

4 of different nociceptor subpopulations.

5 Samples (20 cells per subpopulation and condition) were manually collected using a

6 fire polished pipette with a tip diameter of ~25 µm pulled (Flaming-Brown puller, Sutter

7 Instruments, Novato, CA, USA) from borosilicate glass capillaries (BF150-86-10,

8 Sutter Instrument) that were filled with 2µl of picking buffer [1µL RNAse inhibitor

9 (Takara #2313A) in 49 µL PBS]. After aspirating 20 cells per sample [NGF ±:

10 CHRNA3$^+$, IB4$^-$, IB4$^+$, Aδ-nociceptors (see Fig. 1e); CFA/Saline: CHRNA3-EGFP$^+$/FB$^+$,

11 IB4$^-$/FB$^+$ (see Fig. 3c)] the pipette was immediately shock frozen in liquid Nitrogen and

12 the cells were expelled into an RNAse free tube filled with 8 µL of picking buffer.

13 Directly thereafter, the tubes were stored at -80°C until further processing. For each

14 gene 4 to 9 samples (1 sample per subpopulation and condition per mouse) were

15 collected. Cell populations were identified and picked using a 20x magnification and

16 appropriate filter cubes in the Zeiss Axio Observer A1 microscope (Carl Zeiss). Cell

17 lysis and reverse transcription with cDNA synthesis was carried out directly on the

18 sample using the Power SYBR® Green Cells-to-CT™ Kit (Thermo Fischer Scientific,

19 #4402953) following the manufacturer's instructions. qPCR reactions were set up

20 using FastStart Essential DNA Green Master (Roche, #06402712001) according to the

21 manufacturer's guidelines. Per reaction (20 µl reaction volume) 4 µl of the obtained

22 cDNA as template was added to 10 µl SYBR Green PCR Master Mix, 4 µl nuclease-

23 free H2O and the following forward (FW) and reverse (RV) primer pairs (1µl each of a

24 5µM dilution, final concentration: 250nM): GAPDH-FWD 5'-

25 GCATGGCCTTCCGTGTTC-3'; GAPDH-REV 5'-GTAGCCCAAGATGCCCTTCA-3';

26 TMEM100-FWD 5'-GAAAAACCCCAAGAGGGAAG-3'; TMEM100-REV 5'-

27 ATGGAACCATGGGAATTGAA-3'. qPCR reactions were performed in a LightCycler

28 96 (Roche) with a thermal cycler profile as follows: 10 min preincubation step at 95°C

29 followed by 40 cycles of PCR with a 10 second denaturing cycle at 95°C, followed by

30 10 seconds of annealing at 60ºC and 10 seconds extension at 72°C. Mean ± SEM

31 expression levels of TMEM100 normalized to the expression levels of the

32 housekeeping gene GAPDH were compared in the different nociceptor subclasses

33 cultured in absence and presence of NGF (Fig. 1e). CFA-induced changes in mRNA

34 expression levels of TMEM100 in CHRNA3-EGFP$^+$/FB$^+$ and IB4$^-$/FB$^+$ neurons

1 compared to contralateral control neurons were analyzed using the ΔΔCt method (Fig.

2 3c).

3

4 **RNA Sequencing**

5 For RNAseq, CHRNA3-EGFP$^+$ samples (20 cells per sample and condition) of 3 WT

6 mice were processed, cultured (±NGF for 24h) and collected as described above (see

7 Reverse transcription and quantitative real-time PCR). The SmartSeq2 protocol

8 published by Picelli et al. (2014) was used to process cell lysates to reverse

9 transcription and library preparation was performed using the Nextera DNA Sample

10 Preparation kit (Illumina) following the manufacturer's instructions. Libraries were

11 sequenced with Illumina HiSeq 2000. Sequencing reads were mapped to GRCm38

12 mouse reference genome and differential gene expression analysis was performed

13 using the BioJupies platform [59] with default parameters. Next generation RNA-

14 sequencing raw data (FASTQ files) have been deposited in the Gene Expression

15 Omnibus (GEO) under accession number GSE199580 and are publicly available as of

16 the date of publication.

17

18 **Calcium Imaging**

19 To examine the responsiveness of FB-labelled neurons to the TRPA1 agonist

20 allylisothiocyanate (AITC, Sigma-Aldrich) Calbryte-590 (Calbryte™ 590 AM, AAT

21 Bioquest) Ca^{2+}-imaging was performed. CHRNA3-EGFP$^+$/FB$^+$ neurons and small

22 (<30µm) IB4$^-$/FB$^+$ neurons from both WT and TMEM100KO animals after CFA and

23 control treatment were obtained as described above (see Patch clamp recordings),

24 counterstainded with Alexa Fluor™ -647 conjugated IB4 (2.5µg/ml, Isolectin GS-IB

25 from Griffonia simplicifolia, Alexa Fluor™ 647 Conjugate, Invitrogen™/Thermo Fischer

26 Scientific, I32450) for 10-15 min at room temperature, washed with extracellular buffer

27 (140 mM NaCl, 4 mM KCl, 2 mM $CaCl_2$, 1 mM $MgCl_2$, 4 mM glucose, 10 mM HEPES

28 and was adjusted to pH 7.4 with NaOH) and then incubated with the Ca^{2+} indicator

29 Calbryte-590 (5µM diluted in ECB from a 5 mM stock solution in DMSO) for 30 min at

30 37 °C. Coverslips with loaded cells were then washed with ECB, mounted onto a

31 perfusion chamber and superfused with ECB using a constant laminar flow provided

32 through an 8-channel valve controlled gravity-driven perfusion system (VC3-8xG, ALA

33 Scientific Instruments) and a peristaltic pump. A manifold system with 8 inlet ports fitted

34 to a silicon tube bath inlet whose end was positioned at the outer edge of the coverslip

1   without interfering the visual field was used to provide immediate release of ECB and

2   chemical agents into the superfusion chamber. This system enabled minimal dead

3   volume and air bubbles in the lines. Tubes were identical for each input line. All

4   experiments were conducted at room temperature (23 ± 1 °C). Fluorescence images

5   were captured with a Hamamatsu ORCO-Flash4.0 camera at 2 Hz under an inverted

6   Zeiss Axio Observer A1 microscope equipped with a LED light source (CoolLED pE-

7   340fura). ZEN 2 pro software (Carl Zeiss Microscopy GmbH) was employed to detect

8   and analyze intracellular calcium changes throughout the experiment. During imaging

9   the following protocol was applied. After establishing a 30 s baseline with ECB (0-30

10   s), neurons were challenged with AITC (10 μM) for 60 s (31-90 s) followed by a wash

11   out period of 270 s (91-360 s). At the end of the protocol, 100 mM KCl was applied for

12   30 s (361-390) to depolarize neurons in order to identify viable neurons in contrast to

13   non-neuronal cells or non-functioning neurons. KCl application was followed by a last

14   wash out period with ECB for 30 s (391-420 s). Neuronal viability was defined as a

15   >20% increase of fluorescence intensity from the mean intensity 20 s pre-KCl

16   application (330 -350s).

17   Analysis was conducted by extracting mean intensity values of neurons (CHRNA3-

18   EGFP$^+$/FB$^+$ neurons and IB4$^-$/FB$^+$) after background subtraction from manually drawn

19   regions of interests (ROIs including background ROI) in the ZEN 2 pro software (Carl

20   Zeiss Microscopy GmbH). These values were then transferred into a custom-made

21   Microsoft Excel® template to compute the proportion of neurons responding to AITC

22   under different conditions (CFA/saline; WT/TMEM100KO). In brief, fluorescence is

23   shown as ΔF/F with ΔF = F1 – F (F1 =mean intensity of image, F = mean intensity of

24   baseline fluorescence from 0-20 s). To express percent changes in fluorescence

25   intensity, ΔF was normalized to F and multiplied by 100 (%). Cells responding with an

26   increase > 5 % of fluorescence intensity from baseline to AITC application were

27   counted as AITC responders. Cells not crossing the KCl threshold were excluded from

28   the analysis.

29

30   **Ex-vivo skin-nerve preparation**

31   To examine peripheral sensitization, we directly measured the mechanosensitivity of

32   C-fiber and Aδ-fiber nociceptors in the tibial nerve by recording mechanically evoked

33   action potentials from single nerve fibers in an ex-vivo skin-nerve preparation. To this

34   end, WT and TMEM100KO mice were sacrificed 3d after CFA/saline injection by

1 placing them in a CO2-filled chamber for 2–4 min followed by cervical dislocation. After

2 dissection, the glabrous skin of the hind limb was placed with the corium side up in a

3 heated (32°C) organ bath chamber that was perfused with synthetic interstitial fluid

4 (SIF buffer) consisting of 108 mM NaCl, 3.5 mM KCl, 0.7 mM $MgSO_4$, 26 mM $NaHCO_3$,

5 1.7 mM Na H_2PO_4, 1.5 mM $CaCl_2$, 9.5 mM sodium gluconate, 5.5 mM glucose and 7.5

6 mM sucrose at a pH of 7.4. The tibial nerve was attached in an adjacent chamber for

7 fiber teasing and single-unit recording. As previously described [6], single units were

8 isolated using a mechanical search stimulus applied with a glass rod and classified by

9 conduction velocity, von Frey hair thresholds and adaptation properties to

10 suprathreshold stimuli. A cylindrical metal rod (diameter 1 mm) that was driven by a

11 nanomotor® (MM2A-LS, 914 Kleindiek Nanotechnik GmbH, Germany) coupled to a

12 force measurement system (FMS-LS, Kleindiek Nanotechnik GmbH, Germany) was

13 used to apply mechanical ramp-and-hold stimuli. The mechanical thresholds of single

14 units were determined by mechanically stimulating the most sensitive spot of the

15 receptive fields using von Frey filaments (Aesthesio® Precision Tactile Sensory

16 Evaluators). The force exerted by the weakest von Frey filament that was sufficient to

17 evoke an action potential was considered as the mechanical threshold. The raw

18 electrophysiological data was amplified with an AC coupled differential amplifier

19 (Neurolog NL104 AC), filtered with a notch filter (Neurolog NL125-6), converted into a

20 digital signal with a PowerLab SP4 (ADInstruments) and recorded at a sampling

21 frequency of 20 kHz using LabChart 7.1 (ADInstruments).

22

AAV-PHP.S production

24 AAV-PHP.S viral particles were produced using a modified protocol based on

25 established procedures by Gradinaru and colleagues [60]. Briefly, AAV-293 cells

26 (Agilent, 240073) were seeded on 150mm dishes and transfected using

27 polyethylenimine (Polysciences, 23966) with four plasmids: a pAAV of interest (AAV-

28 CAG-dsRedExpress2 or AAV-CAG-TMEM100-IRES-dsRedExpress2, both with AAV2

29 ITRs), pAdDeltaF6 (Helper, Addgene #112867), pUCmini-iCAP-PHP.S (Addgene

30 #103006) and a mutated pUCmini-iCAP-PHP.S having a 6xHis tag on the VP3 capsid

31 protein [61], with 1:2:2:2 ratio respectively. Cell culture medium was changed at 48 and

32 120 h post-transfection and supernatant containing viral particles was centrifuged at

33 1690 g for 10 minutes. Supernatant medium was filtered (0.2μm) and diluted in PBS.

34 Cell pellet and filtered medium were stored at 4°C. At 120h post transfection, pelleted

1   cells and the ones in the dishes were lysed and incubated at 37°C for 1 hour with the

2   specific PBS buffer containing: MgCl$_2$ 6mM, Triton X-100 0.4%, RNAse A 6µg/ml

3   (Roche, #10109169001), DENARASE 250U/µl (c-LEcta, #20804). Lysed cells were

4   collected, diluted in PBS and centrifuged at 2300 g for 10 minutes. Supernatant from

5   the cell lysate and the filtered medium were incubated separately with equilibrated Ni-

6   sepharose excel histidine-tagged protein purification resin (Cytiva, #17371202) for at

7   least 2 hours at room temperature with gentle mixing. Filtered medium and cell lysate

8   were carefully loaded through a gravity flow chromatography column with a 30µm filter

9   (Econo-pac, Bio Rad, #7321010). Beads were washed with 80ml of washing buffer (20

10   mM imidazole in PBS, pH 7.4) and viral particles were then eluted in 50ml of elution

11   buffer (500 mM imidazole in PBS, pH 7.4). Buffer exchange and concentration was

12   done with Vivaspin 20 ultrafiltration unit having a 1.000.000 molecular weight cut-off

13   (Sartorius). Viral particles were washed and resuspended in PBS and titered using

14   quantitative PCR with primers targeting WPRE element.

15

16 **Statistics**

17   Unless otherwise stated, all data are expressed as means ± s.e.m. All statistical

18   analyses were performed with Microsoft Excel and Prism 9.0 (Graphpad). Data

19   distribution was systematically evaluated using D'Agostino-Pearson test and

20   parametric or non-parametric tests were chosen accordingly. The statistical tests that

21   were used, the exact P-values and information about the number of independent

22   biological replicates are provided in the display items or the corresponding figure

23   legends. Symbols on graphs (* or #) indicate standard P-value range: *, $P < 0.05$; **,

24    $P < 0.01$; ***, $P < 0.001$ and ns (not significant) $P > 0.05$. Additional information about

25   the statistical tests is provided in Data S1 in the Supplementary Information.

26

27 # Data and code availability

28   All data supporting the findings of this study are available within the article and its

29   supplementary information files. All RNA sequencing dataset generated in this study

30   are deposited in the Gene Expression Omnibus under accession number GSE199580.

31   Plasmids generated in this study are available from the corresponding author upon

32   request. Statistical source data are provided with this paper. A reporting summary for

33   this article is available as a Supplementary Information file.

34

References

1. Lewin, G. & Moshourab, R. Mechanosensation and pain. *J Neurobiol* **61**, 30–44 (2004).

2. Zeisel, A. *et al.* Molecular Architecture of the Mouse Nervous System. *Cell* **174**, 999-1014.e22 (2018).

3. Zheng, Y. *et al.* Deep Sequencing of Somatosensory Neurons Reveals Molecular Determinants of Intrinsic Physiological Properties. *Neuron* (2019) doi:10.1016/j.neuron.2019.05.039.

4. Kupari, J. *et al.* Single cell transcriptomics of primate sensory neurons identifies cell types associated with chronic pain. *Nat. Commun.* **12**, 1510 (2021).

5. Renthal, W. *et al.* Transcriptional Reprogramming of Distinct Peripheral Sensory Neuron Subtypes after Axonal Injury. *Neuron* **108**, 128-144.e9 (2020).

6. Arcourt, A. *et al.* Touch Receptor-Derived Sensory Information Alleviates Acute Pain Signaling and Fine-Tunes Nociceptive Reflex Coordination. *Neuron* **93**, 179–193 (2017).

7. Cavanaugh, D. J. *et al.* Distinct subsets of unmyelinated primary sensory fibers mediate behavioral responses to noxious thermal and mechanical stimuli. *Proc. Natl. Acad. Sci.* **106**, 9075–9080 (2009).

8. Huang, T. *et al.* Identifying the pathways required for coping behaviours associated with sustained pain. *Nature* **565**, 86–90 (2019).

9. Dhandapani, R. *et al.* Control of mechanical pain hypersensitivity in mice through ligand-targeted photoablation of TrkB-positive sensory neurons. *Nat. Commun.* **9**, 1640 (2018).

10. MacDonald, D. I. *et al.* Silent cold-sensing neurons contribute to cold allodynia in neuropathic pain. *Brain J. Neurol.* **144**, 1711–1726 (2021).

1   11. Schaible, H. & Schmidt, R. Time course of mechanosensitivity changes in articular

2   afferents during a developing experimental arthritis. *J. Neurophysiol.* **60**, 2180–2195

3   (1988).

4   12. Feng, B. & Gebhart, G. F. Characterization of silent afferents in the pelvic and splanchnic

5   innervations of the mouse colorectum. *Am. J. Physiol. Gastrointest. Liver Physiol.* **300**,

6   G170-80 (2011).

7   13. Sengupta, J. N. & Gebhart, G. F. Characterization of mechanosensitive pelvic nerve

8   afferent fibers innervating the colon of the rat. *J. Neurophysiol.* **71**, 2046–2060 (1994).

9   14. Häbler, H. J., Jänig, W. & Koltzenburg, M. Activation of unmyelinated afferent fibres by

10   mechanical stimuli and inflammation of the urinary bladder in the cat. *J. Physiol.* **425**,

11   545–562 (1990).

12 15. Schmidt, R. *et al.* Novel classes of responsive and unresponsive C nociceptors in human

13   skin. *J. Neurosci.* **15**, 333–341 (1995).

14 16. Gebhart, G. F. Peripheral contributions to visceral hyperalgesia. *Can. J. Gastroenterol. J.*

15   *Can. Gastroenterol.* **13 Suppl A**, 37A-41A (1999).

16 17. Michaelis, M., Häbler, H. J. & Jäenig, W. Silent afferents: a separate class of primary

17   afferents? *Clin. Exp. Pharmacol. Physiol.* **23**, 99–105 (1996).

18 18. Sauerstein, K. *et al.* Low-Frequency Stimulation of Silent Nociceptors Induces Secondary

19   Mechanical Hyperalgesia in Human Skin. *Neuroscience* **387**, 4–12 (2018).

20 19. Prato, V. *et al.* Functional and Molecular Characterization of Mechanoinsensitive "Silent"

21   Nociceptors. *Cell Rep.* **21**, 3102–3115 (2017).

22 20. Poole, K., Herget, R., Lapatsina, L., Ngo, H.-D. & Lewin, G. R. Tuning Piezo ion channels to

23   detect molecular-scale movements relevant for fine touch. *Nat. Commun.* **5**, 3520

24   (2014).

21. Narayanan, P. *et al.* Native Piezo2 Interactomics Identifies Pericentrin as a Novel Regulator of Piezo2 in Somatosensory Neurons. *J. Proteome Res.* **15**, 2676–2687 (2016).

22. Narayanan, P. *et al.* Myotubularin related protein-2 and its phospholipid substrate PIP2control Piezo2-mediated mechanotransduction in peripheral sensory neurons. *eLife* **7**, (2018).

23. Anderson, E. O., Schneider, E. R., Matson, J. D., Gracheva, E. O. & Bagriantsev, S. N. TMEM150C/Tentonin3 Is a Regulator of Mechano-gated Ion Channels. *Cell Rep.* **23**, 701–708 (2018).

24. Wang, J. *et al.* Tethering Piezo channels to the actin cytoskeleton for mechanogating via the cadherin-β-catenin mechanotransduction complex. *Cell Rep.* **38**, (2022).

25. Raouf, R. *et al.* Inhibition of somatosensory mechanotransduction by annexin A6. *Sci. Signal.* **11**, eaao2060 (2018).

26. Zhang, T., Chi, S., Jiang, F., Zhao, Q. & Xiao, B. A protein interaction mechanism for suppressing the mechanosensitive Piezo channels. *Nat. Commun.* **8**, 1797 (2017).

27. Huo, L. *et al.* Piezo2 channel in nodose ganglia neurons is essential in controlling hypertension in a pathway regulated directly by Nedd4-2. *Pharmacol. Res.* **164**, 105391 (2021).

28. Weng, H.-J. *et al.* Tmem100 Is a Regulator of TRPA1-TRPV1 Complex and Contributes to Persistent Pain. *Neuron* **85**, 833–846 (2015).

29. Talavera, K. *et al.* Mammalian Transient Receptor Potential TRPA1 Channels: From Structure to Disease. *Physiol. Rev.* **100**, 725–803 (2020).

30. Amanda H. Lewis & Grandl, J. Stretch and poke stimulation for characterizing mechanically activated ion channels. *Methods Enzymol.* **654**, 225–253 (2021).

1   31. Denk, F., Bennett, D. L. & McMahon, S. B. Nerve Growth Factor and Pain Mechanisms.

2   *Annu. Rev. Neurosci.* **40**, null (2017).

3   32. Montagnoli, C. *et al.* β-NGF and β-NGF receptor upregulation in blood and synovial fluid

4   in osteoarthritis. *Biol. Chem.* **398**, 1045–1054 (2017).

5   33. Wise, B. L., Seidel, M. F. & Lane, N. E. The evolution of nerve growth factor inhibition in

6   clinical medicine. *Nat. Rev. Rheumatol.* **17**, 34–46 (2021).

7   34. Chakrabarti, S. *et al.* Acute inflammation sensitizes knee-innervating sensory neurons

8   and decreases mouse digging behavior in a TRPV1-dependent manner.

9   *Neuropharmacology* **143**, 49–62 (2018).

10 35. Moon, E.-H. *et al.* Generation of mice with a conditional and reporter allele for

11   Tmem100. *Genes. N. Y. N 2000* **48**, 673–678 (2010).

12 36. Agarwal, N., Offermanns, S. & Kuner, R. Conditional gene deletion in primary nociceptive

13   neurons of trigeminal ganglia and dorsal root ganglia. *Genes. N. Y. N 2000* **38**, 122–129

14   (2004).

15 37. Schaefer, I., Prato, V., Arcourt, A., Taberner, F. J. & Lechner, S. G. Differential modulation

16   of voltage-gated sodium channels by nerve growth factor in three major subsets of TrkA-

17   expressing nociceptors. *Mol. Pain* **14**, 1744806918814640 (2018).

18 38. Sandkühler, J. Models and mechanisms of hyperalgesia and allodynia. *Physiol Rev* **89**,

19   707–758 (2009).

20 39. Eitner, A., Hofmann, G. O. & Schaible, H.-G. Mechanisms of Osteoarthritic Pain. Studies

21   in Humans and Experimental Models. *Front. Mol. Neurosci.* **10**, (2017).

22 40. Woolf, C. J. Central sensitization: Implications for the diagnosis and treatment of pain.

23   *Pain* **152**, S2 (2011).

41. Gold, M. S. & Gebhart, G. F. Nociceptor sensitization in pain pathogenesis. *Nat. Med.* **16**, 1248–1257 (2010).

42. Kerstein, P. C., del Camino, D., Moran, M. M. & Stucky, C. L. Pharmacological blockade of TRPA1 inhibits mechanical firing in nociceptors. *Mol. Pain* **5**, 19 (2009).

43. Garrison, S. R. & Stucky, C. L. Contribution of transient receptor potential ankyrin 1 to chronic pain in aged mice with complete Freund's adjuvant-induced arthritis. *Arthritis Rheumatol. Hoboken NJ* **66**, 2380–2390 (2014).

44. Brierley, S. M. *et al.* TRPA1 contributes to specific mechanically activated currents and sensory neuron mechanical hypersensitivity. *J. Physiol.* **589**, 3575–3593 (2011).

45. Vilceanu, D. & Stucky, C. L. TRPA1 Mediates Mechanical Currents in the Plasma Membrane of Mouse Sensory Neurons. *PLoS ONE* **5**, (2010).

46. Zurborg, S., Yurgionas, B., Jira, J. A., Caspani, O. & Heppenstall, P. A. Direct activation of the ion channel TRPA1 by Ca2+. *Nat. Neurosci.* **10**, 277–279 (2007).

47. Richebé, P., Capdevila, X. & Rivat, C. Persistent Postsurgical Pain: Pathophysiology and Preventative Pharmacologic Considerations. *Anesthesiology* **129**, 590–607 (2018).

48. Martindale, J. C., Wilson, A. W., Reeve, A. J., Chessell, I. P. & Headley, P. M. Chronic secondary hypersensitivity of dorsal horn neurones following inflammation of the knee joint. *Pain* **133**, 79–86 (2007).

49. Drake, R. a. R. *et al.* Periaqueductal Grey EP3 Receptors Facilitate Spinal Nociception in Arthritic Secondary Hypersensitivity. *J. Neurosci.* **36**, 9026–9040 (2016).

50. Hsieh, M.-T., Donaldson, L. F. & Lumb, B. M. Differential contributions of A- and C-nociceptors to primary and secondary inflammatory hypersensitivity in the rat. *Pain* **156**, 1074–1083 (2015).

51. Chan, K. Y. *et al.* Engineered AAVs for efficient noninvasive gene delivery to the central and peripheral nervous systems. *Nat. Neurosci.* **20**, 1172–1179 (2017).

52. Murthy, S. E. *et al.* The mechanosensitive ion channel Piezo2 mediates sensitivity to mechanical pain in mice. *Sci. Transl. Med.* **10**, (2018).

53. Krug, H. E., Dorman, C., Blanshan, N., Frizelle, S. & Mahowald, M. Spontaneous and Evoked Measures of Pain in Murine Models of Monoarticular Knee Pain. *J. Vis. Exp. JoVE* (2019) doi:10.3791/59024.

54. Nees, T. A. *et al.* Early-onset treadmill training reduces mechanical allodynia and modulates calcitonin gene-related peptide fiber density in lamina III/IV in a mouse model of spinal cord contusion injury. *Pain* **157**, 687–697 (2016).

55. Hargreaves, K., Dubner, R., Brown, F., Flores, C. & Joris, J. A new and sensitive method for measuring thermal nociception in cutaneous hyperalgesia. *Pain* **32**, 77–88 (1988).

56. Lechner, S. G. & Lewin, G. R. Peripheral sensitisation of nociceptors via G-protein-dependent potentiation of mechanotransduction currents. *J. Physiol.* **587**, 3493–3503 (2009).

57. Obeidat, A. M., Miller, R. E., Miller, R. J. & Malfait, A.-M. The nociceptive innervation of the normal and osteoarthritic mouse knee. *Osteoarthritis Cartilage* **27**, 1669–1679 (2019).

58. Picelli, S. *et al.* Full-length RNA-seq from single cells using Smart-seq2. *Nat. Protoc.* **9**, 171–181 (2014).

59. Torre, D., Lachmann, A. & Ma'ayan, A. BioJupies: Automated Generation of Interactive Notebooks for RNA-Seq Data Analysis in the Cloud. *Cell Syst.* **7**, 556-561.e3 (2018).

60. Challis, R. C. *et al.* Systemic AAV vectors for widespread and targeted gene delivery in rodents. *Nat. Protoc.* **14**, 379–414 (2019).

61. Zhang, H.-G. *et al.* Addition of six-His-tagged peptide to the C terminus of adeno-associated virus VP3 does not affect viral tropism or production. *J. Virol.* **76**, 12023–12031 (2002).

Acknowledgements

Author Contributions

T.A.N., N.W., C.V., P.A., I.S., S.B., J.V., V.P., C.M., N.Z., F.J.T. and S.G.L. performed the experiments and analyzed data. G.R.L., Y.J.L. and P.A.H. provided material. T.A.N. and S.G.L. designed and supervised the experiments and wrote the manuscript.

Competing interests

The authors declare no competing interests

Figures
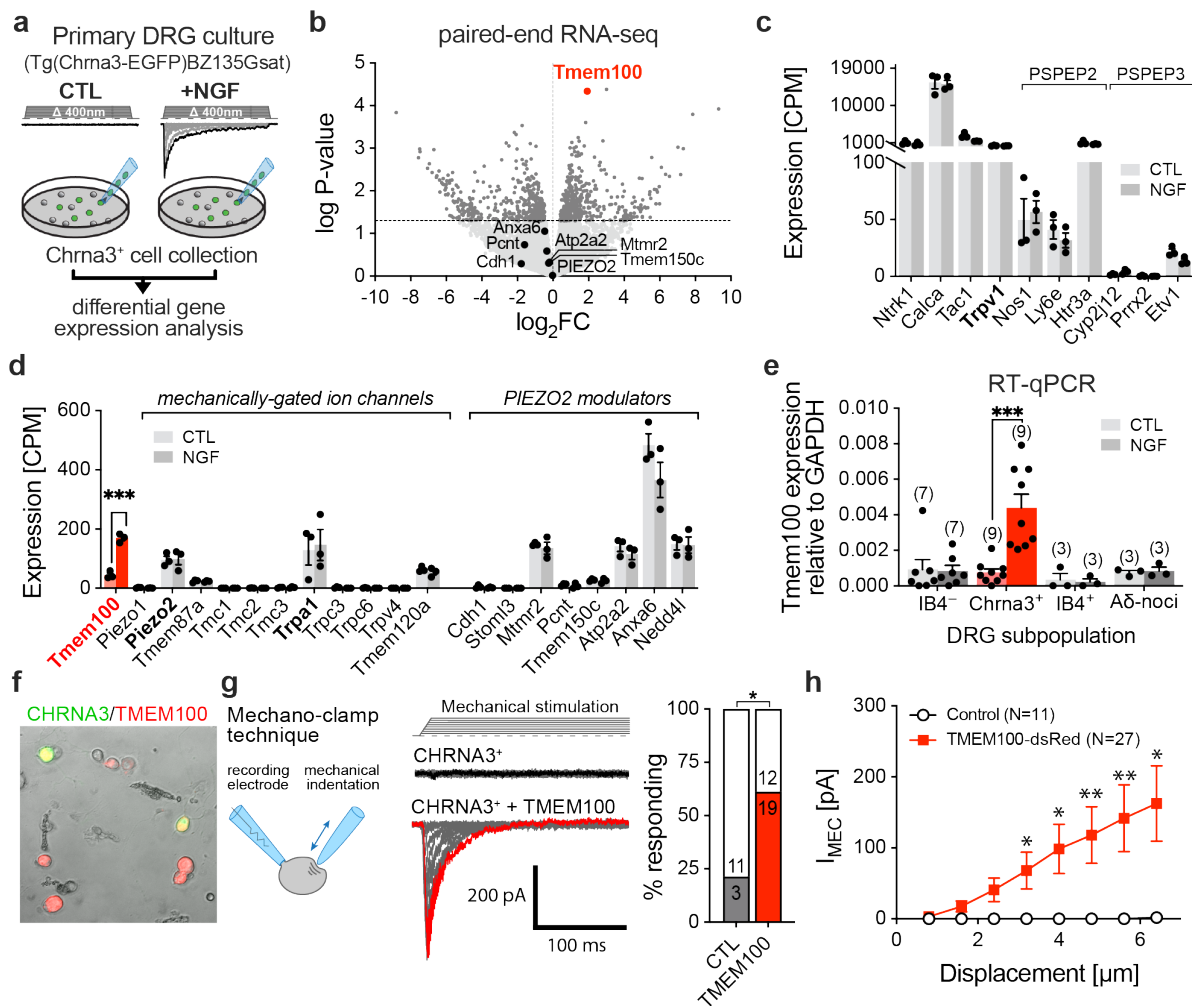
Fig. 1 NGF treatment selectively upregulates TMEM100 in silent nociceptors.
a, Cartoon depicting the experimental design of the RNAseq screen. Cultured CHRNA3-EGFP$^+$ DRG neurons, which acquire mechanotransduction currents upon NGF treatment (top traces), were collected by aspiration into a patch-pipette and subsequently processed for RNA sequencing. **b,** Volcano plot showing the mean fold change of expression (log$_2$FC) vs. the log P-Value (N = 3 samples per condition; 20 cells per sample, Student's T-test). **c**, Comparison of the expression levels (counts per million, CPM) of peptidergic nociceptor subclass markers and **d** mechanically-gated ion channels and PIEZO2 modulators, determined by RNAseq in CHRNA3-EGFP$^+$ neurons culture with and without NGF. **e,** Comparison of the mean ± SEM expression levels of TMEM100 normalized to the expression levels of the housekeeping gene GAPDH in the indicated nociceptor subclasses, cultured in the absence and presence of NGF. To enable identification of peptidergic C-fiber nociceptors, non-peptidergic C-fiber nociceptors and Aδ-fiber nociceptors for sample collection, cultures were prepared from Tg(Npy2r-cre)SM19Gsat/Mmucd x B6;129S-Gt(ROSA)26Sortm32(CAG-COP4*H134R/EYFP)Hze/J (Npy2r^{Cre};ChR2-EYFP) mice, in which Aδ-fiber nociceptors express EYFP and were additionally labelled with Alex-Fluor-568 conjugated Isolectin B4 (IB4), which selectively binds to non-peptidergic C-fiber nociceptors. Numbers of samples (20 cells each) per cell type are indicated above the bars and individual values are shown as black dots (Mann-Whitney test: ns, P>0.05, ***, P=0.000082). **f,** Image showing cultured DRG neurons from CHRNA3-EGFP mice transfected with TMEM100-dsRed. **g,** Cartoon depicting the mechano-clamp configuration of the patch clamp technique (left), example traces of mechanically-evoked currents in CHRNA3-EGFP$^+$ control cells (middle, top) and in TMEM100-dsRed transfected CHRNA3-EGFP$^+$ cells (middle, bottom) as well as bar graph showing the proportion of cells responding to mechanical stimulation. Proportions were compared with Fisher's exact test. (P=0.023). **h,** Mean ± SEM peak amplitudes of mechanically-evoked currents are shown as a function of membrane displacement for control (white circles) and TMEM100 transfected cells (red squares). Current amplitudes were compared using multiple Mann-Whitney tests (*, P<0.05; **, P<0.01). N-numbers differ from **g**, because some recordings crashed before maximal mechanical stimulation. Source data and statistical information are provided as a Source Data file.
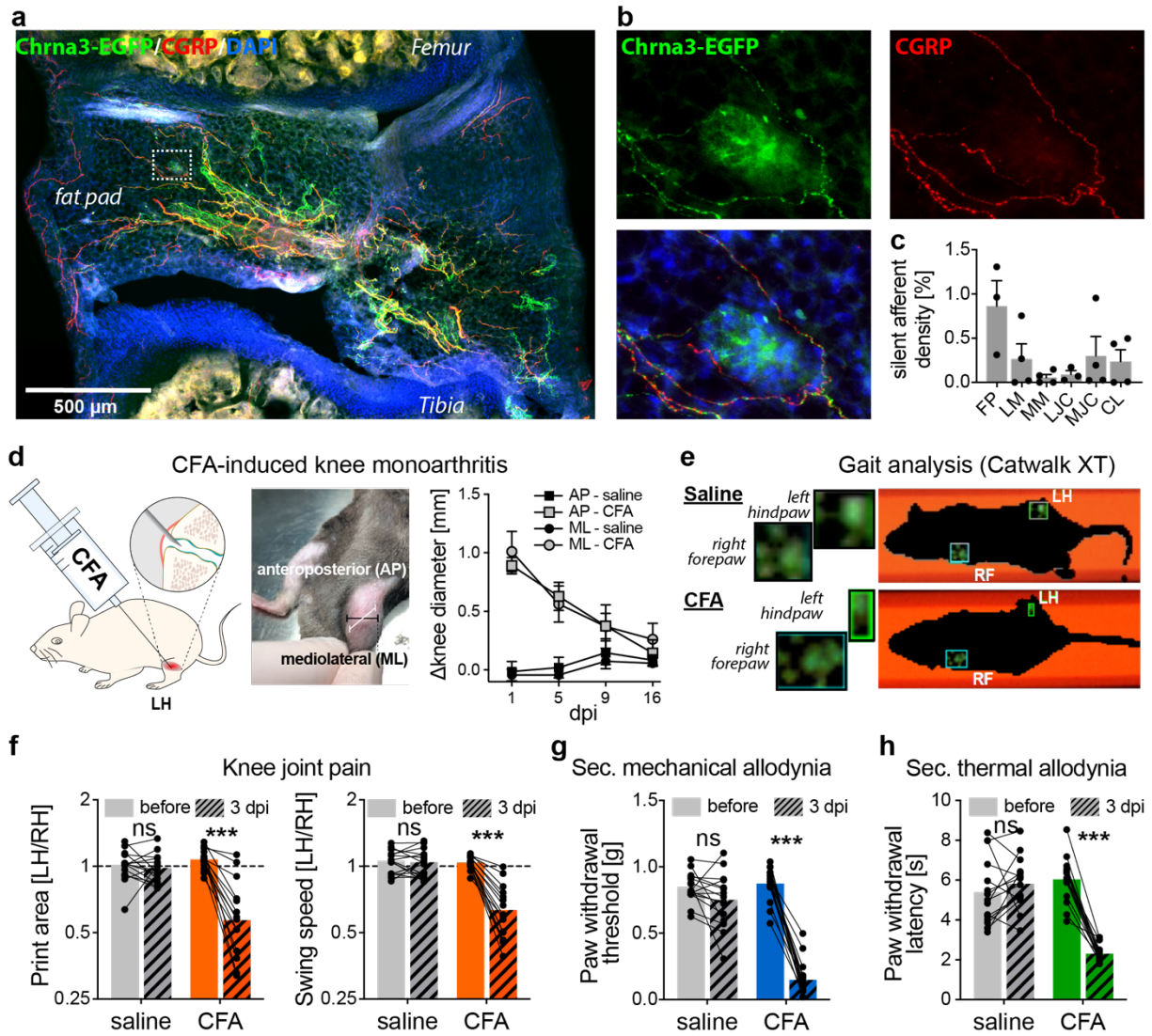
36

Fig. 2 Intraarticular CFA injection induces knee joint pain and secondary allodynia in the hind paw.

a, Representative image of a knee joint section immunostained for CGRP and EGFP to enhance the endogenous EGFP signal of CHRNA3+ afferents. Note, only EGFP+ fibers that co-express CGRP are sensory afferents. CGRP–/EGFP+ fibers are sympathetic efferents (see Prato et al., 2017). **b,** Close-up of the region marked by the white rectangle in (A), emphasizing co-expression of EGFP and CGRP. **c,** Quantification of silent afferent density (EGFP+/CGRP+ fibers) in anatomically defined regions. FP (Hoffa's fat pad), LM (lateral meniscus), MM (medial meniscus), LJC (lateral joint capsule), MJC (medial joint capsule), CL (cruciate ligament). Bars represent means ± SEM from three different mice. Individual values from each mouse are shown as black dots. **d,** Cartoon depicting the experimental approach (left), photograph of an inflamed knee (middle) and time course (days post-injection, dpi) of the inflammation-induced knee swelling (right). **e,** Freeze frames of Catwalk XT movies from saline (top) and CFA (bottom) treated mice. Note, CFA-treated mice only put little weight on the left hind paw (small foot print). **f,** Comparison of the foot print area ratio (left/right hindpaw; LH/RH) and the leg swing time ratio (LH/RH) measured before (solid bars) and three day after (3 dpi, hatched bars) saline (grey) and CFA (orange) injection. Paired Student's t-test (saline N=15, CFA N=16; print area CFA, $P = 2.6*10^{-7}$; swing speed CFA $P=8*10^{-9}$). **g,** Comparison of mechanical paw withdrawal thresholds before (solid bars) and three day after (3 dpi, hatched bars) saline (grey) and CFA (blue) injection. Paired Student's t-test (saline N=15, CFA N=16; CFA, $P = 5.18*10^{-12}$). **h,** Comparison of thermal paw withdrawal latencies before (solid bars) and three day after (3 dpi, hatched bars) saline (grey) and CFA (blue) injection. Paired Student's t-test (saline N=15, CFA N=16; CFA, $P = 1.8*10^{-9}$). Source data and statistical information are provided as a Source Data file.

37
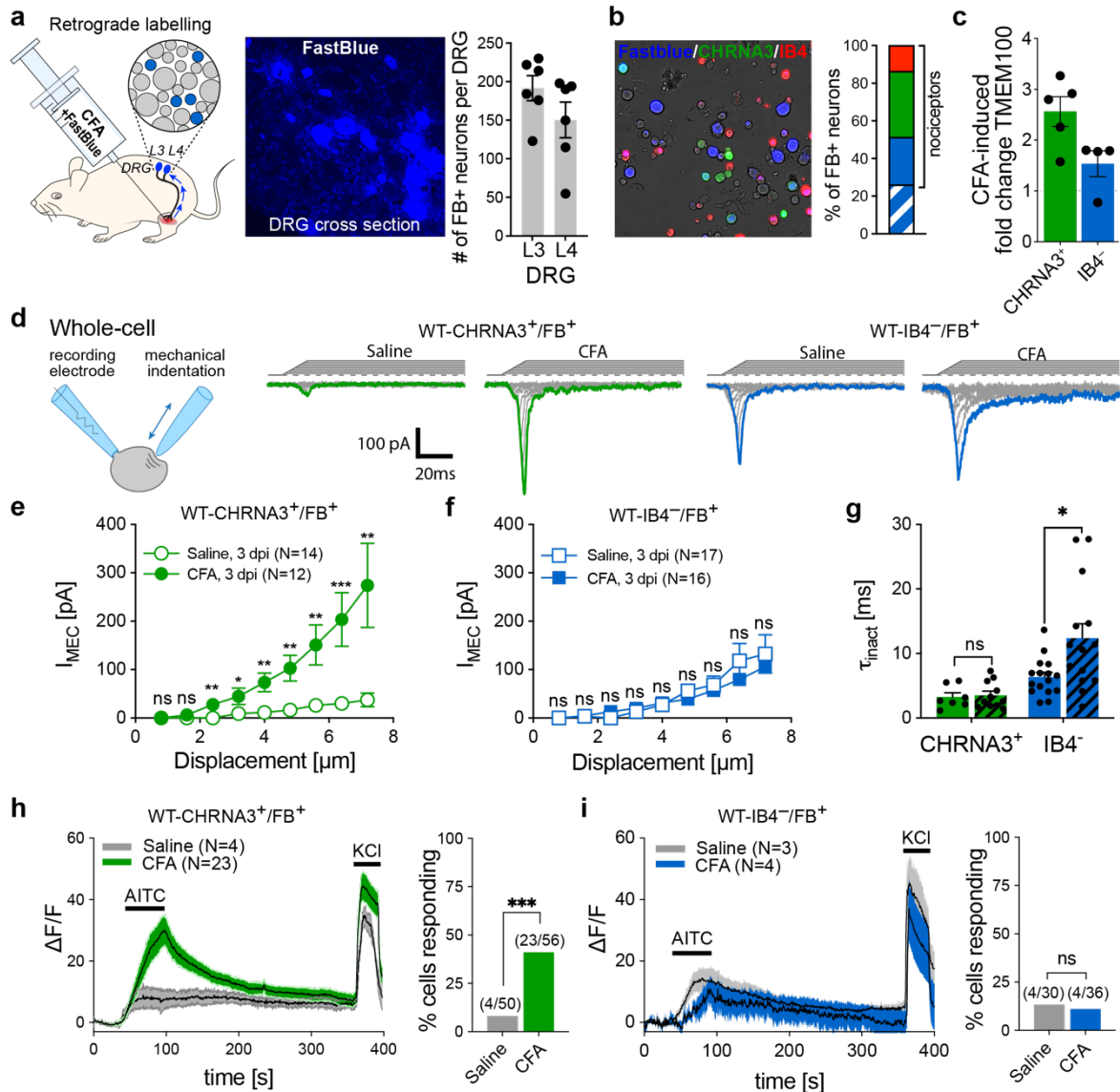
Fig. 3 CFA-induced knee joint inflammation induces mechanosensitivity and potentiates TRPA1 activity in CHRNA3-EGFP⁺ afferents.

a, Cartoon depicting the retrograde labeling approach of knee joint afferents (left), example image of fast blue positive neurons in a DRG cross section (middle) and quantification of the total number of FB⁺ neurons in L3 and L4 DRGs from 6 mice. Bars represent means ± SEM and individual values for each DRG are shown as black dots. **b,** Example image of a primary DRG culture from a CHRNA3-EGFP mouse that had received intraarticular FB (left). The stacked bar graph (right) shows the proportions of IB4⁺ cells (non-peptidergic nociceptors, red), MIAs (green), peptidergic nociceptors (IB4⁻, < 30μm, blue) and group II articular afferents (IB4⁻, >30μm, blue hatched). **c,** Quantification of CFA-induced changes in TMEM100 expression in retrogradely labelled MIAs and peptidergic nociceptors. Expression levels in ipsi- and contralateral DRGs were determined by qPCR and compared using the ΔΔCt method. **d,** Cartoon depicting the mechano-clamp configuration of the patch clamp technique (left) and example traces of mechanically-evoked currents in the indicated cell types and conditions (right). **e** and **f** Peak amplitudes of mechanically-evoked currents are shown as a function of membrane displacement for **e** MIAs and **f** peptidergic nociceptors from saline (open symbols) and CFA-treated (solid symbols) mice. Current amplitudes were compared using Mann-Whitney test (*, P<0.05; **, P<0.01; ***, P<0.001; ns, P>0.05). **g,** Comparison of the inactivation time constants of the mechanically evoked currents determined with single exponential fit. Bars represent means ± SEM and individual values are shown as black dots. **h** and **i** Time course of changes in the intracellular Ca²⁺ concentration determined with Calbryte-590 Ca²⁺ imaging (left) of **h** retrogradely labelled MIAs and **i** peptidergic nociceptors from saline and CFA treated mice, responding to 10 μM AITC and 100 mM KCl and bar graphs (right) showing the proportion of cells that responded to AITC. N-numbers are provided in the graph legends. Proportions were compared with Fishers exact test. ns, not significant; ***, P=0.000102. Source data and statistical information are provided as a Source Data file.
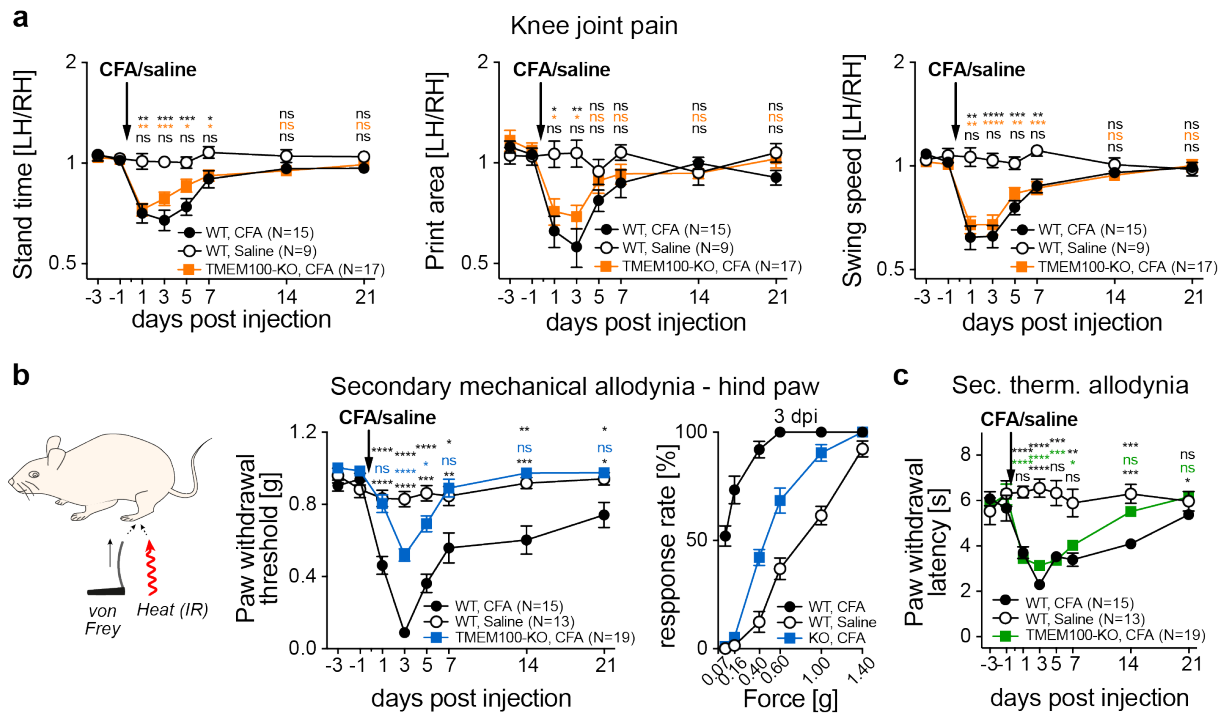
Fig. 4 TMEM100 knock-out mice develop normal inflammatory knee joint pain but no long-lasting secondary mechanical allodynia.

a, Comparison of the time courses of changes in stand time (left), foot print area (middle) and leg swing speed (right) of saline injected WT mice (white circles), CFA injected WT mice (black circles) and CFA injected TMEM100KO mice (orange squares). **b**, Cartoon depicting the experimental approach for measuring secondary mechanical and thermal hypersensitivity in the ipsilateral hindpaw (left), time courses of changes in mechanical paw withdrawal thresholds of saline injected WT mice (white circles), CFA injected WT mice (black circles) and CFA injected TMEM100KO mice (blue squares) (middle) and responsiveness of WT mice (white circles), CFA injected WT mice (black circles) and CFA injected TMEM100KO mice (blue squares) three days post saline/CFA injection (3 dpi) to all tested von Frey filaments (right). Response rates were compared using 2-way ANOVA. P-values of multiple comparisons are as follows: WT-saline vs. WT-CFA, $P_{0.07g}$ = 7.5E-08, $P_{0.16g}$ = 2.8E-08, $P_{0.4g}$ = 8.7E-12, $P_{0.6g}$ = 7.5E-08, P_{1g} = 2.6E-06, $P_{1.4g}$ = 1.2E-01; WT-saline vs. TMEM100KO-CFA, $P_{0.07g}$ = 5.9E-01, $P_{0.16g}$ = 3.3E-01, $P_{0.4g}$ = 1.5E-04, $P_{0.6g}$ = 7.8E-04, P_{1g} = 6.8E-05, $P_{1.4g}$ = 1.2E-01; WT-CFA vs. TMEM100KO-CFA, $P_{0.07g}$ = 5.2E-08, $P_{0.16g}$ = 3.6E-08, $P_{0.4g}$ = 3.9E-10, $P_{0.6g}$ = 9.9E-05, P_{1g} = 6.1E-02, $P_{1.4g}$ = not determined). **c,** Time courses of changes in thermal paw withdrawal latencies of saline injected WT mice (white circles), CFA injected WT mice (black circles) and CFA injected TMEM100KO mice (green squares). **a** – **c** Symbols represent means ± SEM. Unless otherwise stated, ratios at different time points were compared using mixed model ANOVA and P-values of multiple comparisons are indicated above the white circles. Top, WT-saline vs. WT-CFA; middle, WT-saline vs. TMEM100KO-CFA; bottom, WT-CFA vs. TMEM100KO-CFA (*, P < 0.05; **, P < 0.01; ***, P < 0.001; ns, P > 0.05, N-numbers are provided in the graph legends). Source data and statistical information are provided as a Source Data file.
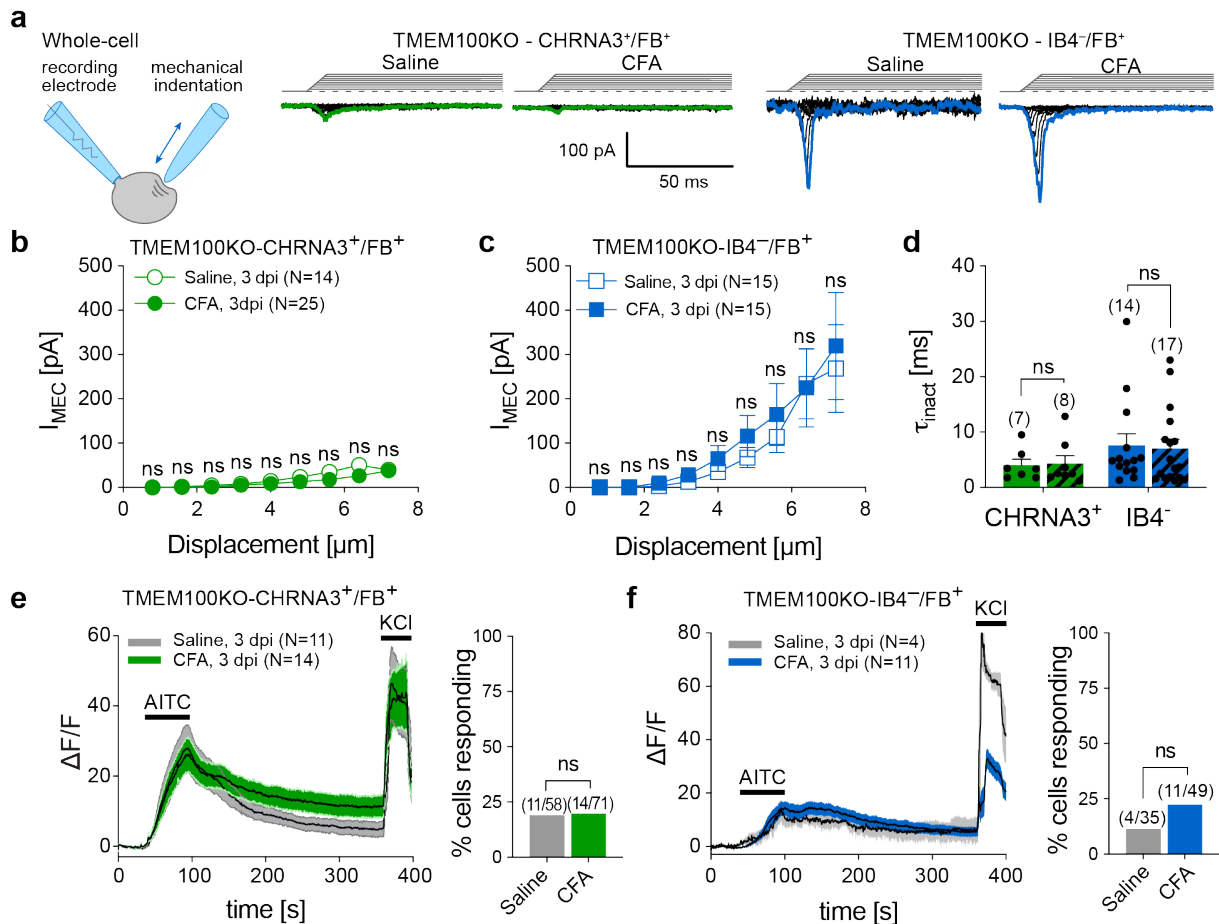
Fig. 5. CFA-induced knee joint inflammation fails to sensitize CHRNA3-EGFP$^+$ neurons to mechanical stimuli in TMEM100 knock-out mice.

a, Cartoon depicting the mechano-clamp configuration of the patch clamp technique (left) and example traces of mechanically-evoked currents in the indicated cell types and conditions (right). Note, in contrast to WT mice, CHRNA3-EGFP$^+$ neurons from TMEM100KO mice do not acquire mechanosensitivity during CFA-induced inflammation. **b** and **c** Peak amplitudes of mechanically-evoked currents are shown as a function of membrane displacement for **b** MIAs and **c** peptidergic nociceptors from saline (open symbols) and CFA-treated (solid symbols) mice. Current amplitudes were compared using Mann-Whitney test (ns, P>0.05). **d,** Comparison of the inactivation time constants of the mechanically evoked currents determined with single exponential fit. Bars represent means ± SEM and individual values are shown as black dots. **e** and **f** Time course of changes in the intracellular Ca^{2+} concentration determined with Calbryte-590 Ca^{2+} imaging (left) of retrogradely labelled **e** MIAs and **f** peptidergic nociceptors from saline (grey) and CFA (green) treated mice, challenged with 10 µM AITC and 100 mM KCl and bar graphs (right) showing the proportion of cells that responded to AITC. N-numbers are provided in the graph legends. Proportions were compared with Fishers exact test (ns, not significant). Black lines represent means and grey and green shaded areas represent SEM. Source data and statistical information are provided as a Source Data file.
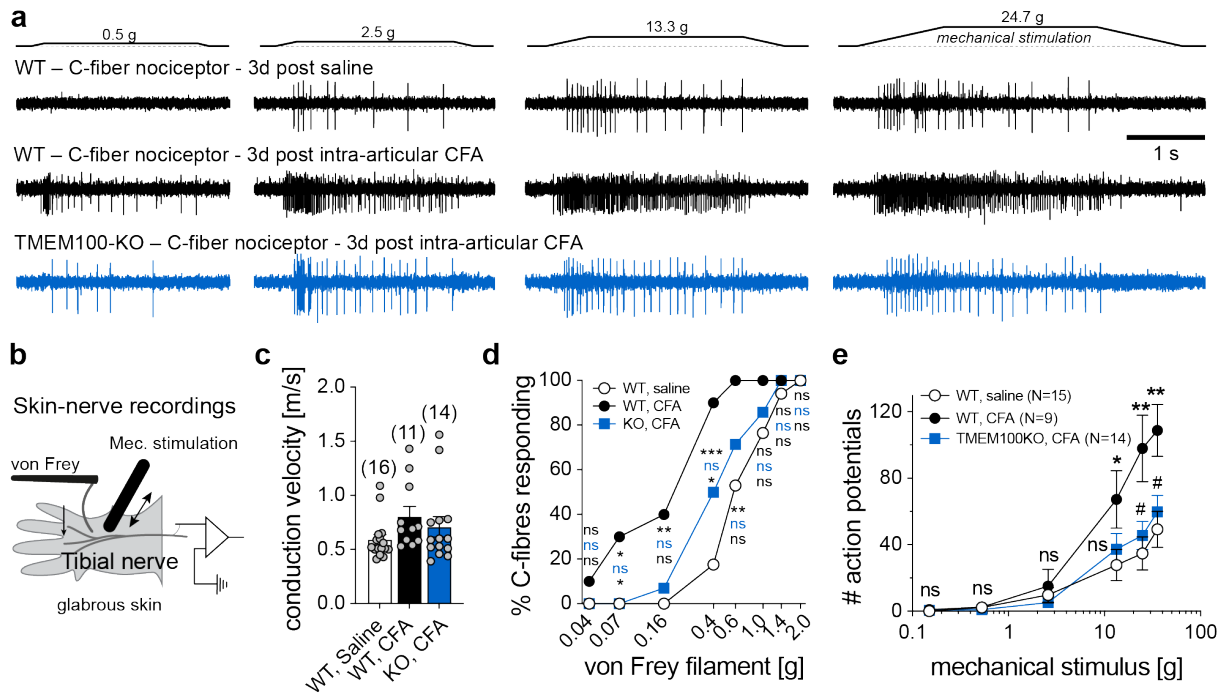
Fig. 6 Sensitization of cutaneous C-fiber nociceptors contributes to secondary mechanical allodynia.

a, Example traces of mechanically-evoked action potentials recorded from single nerve fibers from the tibial nerve of WT mice 3 days post intraarticular saline (top), WT mice 3 dpi CFA (middle) and TMEM100KO mice 3 dpi CFA (bottom). **b,** Cartoon depicting the experimental approach. **c,** Scatter dot plots of the conduction velocities [m/s] of the examined afferent fibers from the indicated mice. Bars represent means ± SEM. **d,** Comparison of the proportions of C-fiber nociceptors that respond to mechanical stimulation with the indicated von Frey filaments. The proportions were compared pairwise using the Chi-square test. P-values are provided next to the symbols in the graph and refer to WT-saline vs. WT-CFA (top, black), WT-saline vs. TMEM100KO-CFA (middle, blue) and WT-CFA vs. TMEM100KO (bottom, black). N-numbers are the same as in (C). **e,** Comparison of the firing rates evoked by a series of ramp-and-hold stimuli with increasing amplitudes that exerted the indicated force to the receptive fields. Symbols represent the mean ± SEM numbers of action potentials, which were compared using multiple Mann-Whitney tests. (WT-saline vs. WT-CFA: *, P<0.05; **, P<0.01; WT-CFA vs. TMEM100KO-CFA: #, P<0.05). Source data and statistical information are provided as a Source Data file.
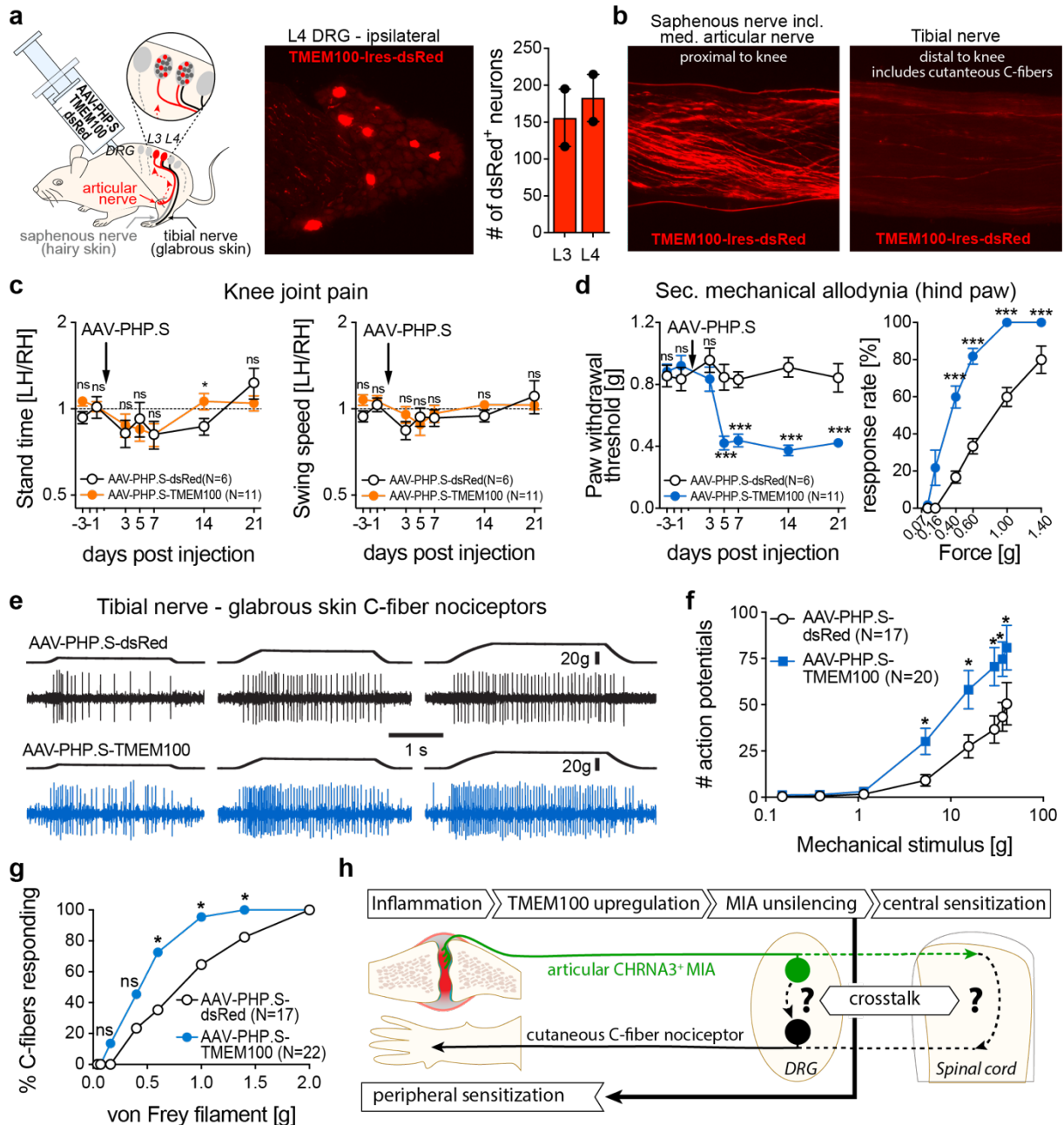
41

Fig. 7 Overexpression of TMEM100 in articular afferents induces secondary allodynia in the hind paw but no knee joint pain.

a, Cartoon depicting the experimental approach (left), example image of a DRG cross section from a mouse that had received intraarticular AAV-PHP.S-TMEM100-Ires-dsRed (middle) and quantification of the total number of dsRed+ neurons (right). Bars represent means ± SEM and values from individual DRGs are shown as black dots. **b,** dsRed fluorescence in the tibial nerve distal to the knee (left) and the saphenous (right) nerve proximal to the knee which contains the medial articular nerve. **c,** comparison of the time courses of changes in stand time (left) and leg swing speed (right) of WT mice that intraarticularly received AAV-PHP.S-dsRed control virus (white circles) and AAV-PHP-S-TMEM100-Ires-dsRed (orange circles). Ratios at different time points were compared using multiple Mann-Whitney tests. (ns, P>0.05; *, P<0.05; N-numbers are provided in the graph legend). **d,** Time courses of changes in mechanical paw withdrawal thresholds of AAV-PHP.S-dsRed (white circles) and AAV-PHP-S-TMEM100-Ires-dsRed (blue circles) injected WT mice (left) as well as comparison of the response rates at different time points were compared using Mann-Whitney test (***, P<0.001; number of tested animals is the same in both panels and is indicated in the graph legend). **e,** Example traces of mechanically-evoked action potentials recorded from cutaneous C-fiber nociceptors in the tibial nerve

1 from control mice (top, AAV-PHP.S-dsRed) and from mice that overexpress TMEM100 in articular
2 afferents (bottom, AAV-PHP.S-TMEM100-Ires-dsRed). **f,** comparison of the firing rates evoked by ramp-
3 and-hold stimuli that exerted the indicated force to the receptive fields. Symbols represent means ± SEM
4 numbers of action potentials, which were compared using multiple Mann-Whitney tests (*, P<0.05). **g,**
5 comparison of the proportions of C-fiber nociceptors that respond to mechanical stimulation with the
6 indicated von Frey filaments. The proportions were compared pairwise using the Chi-square test (ns,
7 not significant; *, P<0.05). **h,** cartoon depicting the proposed mechanism underlying the induction of
8 secondary hypersensitivity. Source data and statistical information are provided as a Source Data file.